NASA/TM—2010-216260

Moisture-Induced Alumina Scale Spallation: The Hydrogen Factor

James L. Smialek
Glenn Research Center, Cleveland, Ohio

April 2010

NASA STI Program . . . in Profile

Since its founding, NASA has been dedicated to the advancement of aeronautics and space science. The NASA Scientific and Technical Information (STI) program plays a key part in helping NASA maintain this important role.

The NASA STI Program operates under the auspices of the Agency Chief Information Officer. It collects, organizes, provides for archiving, and disseminates NASA's STI. The NASA STI program provides access to the NASA Aeronautics and Space Database and its public interface, the NASA Technical Reports Server, thus providing one of the largest collections of aeronautical and space science STI in the world. Results are published in both non-NASA channels and by NASA in the NASA STI Report Series, which includes the following report types:

- TECHNICAL PUBLICATION. Reports of completed research or a major significant phase of research that present the results of NASA programs and include extensive data or theoretical analysis. Includes compilations of significant scientific and technical data and information deemed to be of continuing reference value. NASA counterpart of peer-reviewed formal professional papers but has less stringent limitations on manuscript length and extent of graphic presentations.

- TECHNICAL MEMORANDUM. Scientific and technical findings that are preliminary or of specialized interest, e.g., quick release reports, working papers, and bibliographies that contain minimal annotation. Does not contain extensive analysis.

- CONTRACTOR REPORT. Scientific and technical findings by NASA-sponsored contractors and grantees.

- CONFERENCE PUBLICATION. Collected papers from scientific and technical conferences, symposia, seminars, or other meetings sponsored or cosponsored by NASA.

- SPECIAL PUBLICATION. Scientific, technical, or historical information from NASA programs, projects, and missions, often concerned with subjects having substantial public interest.

- TECHNICAL TRANSLATION. English-language translations of foreign scientific and technical material pertinent to NASA's mission.

Specialized services also include creating custom thesauri, building customized databases, organizing and publishing research results.

For more information about the NASA STI program, see the following:

- Access the NASA STI program home page at *http://www.sti.nasa.gov*

- E-mail your question via the Internet to *help@sti.nasa.gov*

- Fax your question to the NASA STI Help Desk at 443–757–5803

- Telephone the NASA STI Help Desk at 443–757–5802

- Write to:
  NASA Center for AeroSpace Information (CASI)
  7115 Standard Drive
  Hanover, MD 21076–1320

NASA/TM—2010-216260

Moisture-Induced Alumina Scale Spallation: The Hydrogen Factor

James L. Smialek
Glenn Research Center, Cleveland, Ohio

National Aeronautics and
Space Administration

Glenn Research Center
Cleveland, Ohio 44135

April 2010

Acknowledgments

This work was funded under the NASA Fundamental Aeronautics Program. Professor N. Leventis is acknowledged for obtaining Rene N5 baseline polarization curves against a Ag/AgCl standard electrode, and Professor S. Hayashi is acknowledged for performing GDOES hydrogen profiles for moisture-treated pre-oxidized Rene N5 samples. Helpful comments on special issues from G. Hultquist, J.R. Smith, R. Hayes, N. Leventis, T. Gabb, and S. Hayashi are gratefully appreciated. Figures 7, 13, 14, 15, 21, and 26 are reprinted with permission from the publishers (JOM, Springer, Elsevier, and DECHEMA).

This work was sponsored by the Fundamental Aeronautics Program at the NASA Glenn Research Center.

Level of Review: This material has been technically reviewed by technical management.

Available from

NASA Center for Aerospace Information
7115 Standard Drive
Hanover, MD 21076–1320

National Technical Information Service
5301 Shawnee Road
Alexandria, VA 22312

Available electronically at http://gltrs.grc.nasa.gov

Moisture-Induced Alumina Scale Spallation: The Hydrogen Factor

James L. Smialek
National Aeronautics and Space Administration
Glenn Research Center
Cleveland, Ohio 44135

Abstract

For some time the oxidation community has been concerned with interfacial spallation of protective alumina scales, not just upon immediate cool down, but as a time-delayed phenomenon. Moisture-induced delayed spallation (MIDS) and desktop spallation (DTS) of thermal barrier coatings (TBCs) refer to this process. It is most apparent for relatively adherent alumina scales that have survived initial cool down in a dry environment, have built up considerable thickness and strain energy, and have been somewhat damaged, such as by cyclic oxidation cracking. Indeed, a "sensitive zone" can be described that maximizes the observed effect as a function of all the relevant factors. Moisture has been postulated to serve as a source of interfacial hydrogen embrittlement. Hydrogen is derived from reaction with aluminum in the alloy at an exposed interface. The purpose of this monograph is to trace the close analogy of this phenomenon to other hydrogen-induced effects, such as embrittlement of aluminides and blistering of alloys and anodic alumina films. A formalized, top-down, logic-tree structure is presented as a guide to this discussion. A theoretical basis for interfacial weakening by hydrogen is first cited, as are demonstrations of hydrogen detection as a reaction product or interfacial species. Further support is provided by critical experiments that recreate the moisture effect, but by isolating hydrogen from other potential causative factors. These experiments include tests in H_2-containing atmospheres or cathodic hydrogen charging. Accordingly, they strongly indicate that interfacial hydrogen, derived from moisture, is the key chemical species accounting for delayed alumina scale spallation.

Introduction

There are numerous reported instances of moisture-induced spallation of alumina scales formed by high temperature oxidation. These occur under ambient conditions and are often discussed in terms of analogous moisture-induced phenomena for clarification of the hypothetical mechanism. Accordingly, it has been proposed that hydrogen, as a by-product of a room temperature moisture-alloy reaction, plays a key role in triggering spallation by affecting the interfacial scale-metal strength (Refs. 1 and 2). Such an effect is not at all unexpected considering ab initio models and interfacial toughness measurements that include hydrogen effects. Many similar attributes of hydrogen-related phenomena are sited as circumstantial evidence for this scale spallation mechanism, including hydrogen embrittlement of aluminides and blistering of anodic scales. The details of these supporting phenomena are not always fully presented. Furthermore, inductive arguments have generally been presented from the bottom up, citing scale spallation phenomenology, then generalizing to an overriding principal. It is the purpose of this monograph to present a deductive argument, restructured from the top down. We start with general principals, show parallels of several similar phenomena, and elaborate somewhat on the supporting evidence in each specific case. The intent is to present the proposed mechanism from a broader, more formalized perspective. Due in part to the analytical challenge, direct identification of the hydrogen factor is problematic. Thus, in a sense, relevant information has been gathered from widely disparate fields, to produce a patchwork of unusual, if not oddly related results. But they are brought together toward a common theme, gathering synergistic, cumulative support. In the end, a mosaic of interrelated phenomena is interwoven to form a coherent argument. Hopefully, this structured framework may point the way toward more revealing experiments that not only test the basic hypotheses, but also elaborate on some atomistic details. In time, this new direction could provide a logical description of a more precise hydrogen factor.

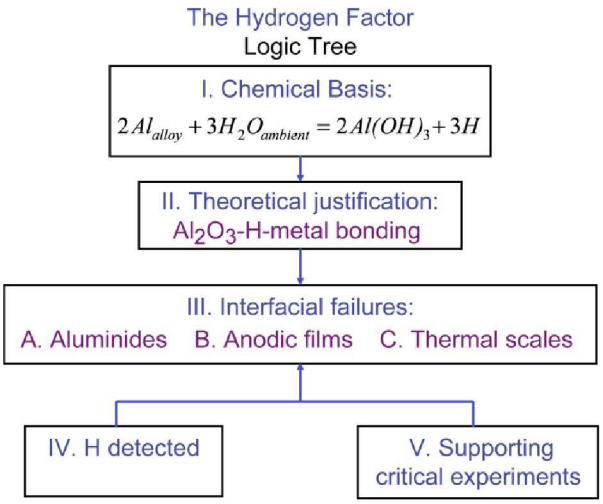

Figure 1.—Conceptual outline showing top-down logic structure for the proposed hydrogen effect in moisture induced delayed spallation of alumina scales.

The basic elements and guide are provided in the schematic entitled "The Hydrogen Factor: Logic Tree," (Fig. 1). The implied argument is that the MIDS and DTS phenomena follow from a logical flow of basic reaction chemistry and interfacial bonding theory. The similarities and analogies to other related phenomena provide the hypothesis that one single mechanism applies across the board. The case is strengthened or, in some cases, proven by actual detection of interfacial hydrogen and elimination of all other factors except hydrogen. According to this scheme, we first try to justify (I) the generation of hydrogen from moisture in the presence of transition metals. Then (II) theoretical results for the detrimental effects of hydrogen on the strength of the alumina-metal bond are presented. A number of analogous phenomenological observations (III), believed to derive from these same premises, are compared. Two factors of support are offered as proofs for each of the phenomena: (IV) the detection of hydrogen at the weakened interface and (V) critical experiments isolating hydrogen effects from other possible ambient factors. This basic outline will be followed after presenting the attributes of both hydrogen embrittlement and moisture-induced spallation.

The intent is to assemble a chain of evidence from apparently disparate, but actually quite substantively, related fields that, by analogy, identifies hydrogen as the key factor. In a sense, the same had been done for sulfur effects on scale adhesion, where striking similarities existed with sulfur segregation and grain boundary embrittlement of transition metals. In that case, the telling experiment was the retarding effect of Y on the surface segregation of sulfur for NiCrAl(Y) oxidation resistant coatings. From here, studies of the effect of sulfur content on spallation and, eventually, direct observations of interfacial sulfur confirmed the hypothesis. In the case of hydrogen, the luxury of direct observation by conventional techniques does not currently exist. So the purpose of this paper is to assemble the evidence from related studies to provide an impetus for this new line of research. The telling experiments, conclusively identifying interfacial hydrogen from exposure to moisture, are imminent, but remain an embryonic area of endeavor.

General Attributes of Hydrogen Embrittlement

Hydrogen embrittlement has been a widespread metallurgical issue for the better part of a century. Accordingly, it has received an enormous amount of attention, from both the application and fundamental mechanism arenas. For the present purposes, it will suffice to highlight the most common attributes of the phenomenon, which can be found in any review or treatise on the subject.

Often an aqueous exposure is involved. This allows for global (e.g., galvanic) or local (pitting) electrochemical cells to produce a (-) cathodic driving force, attracting H^+ ions. As such, it is often enhanced by acidic conditions and sometimes found in cases of pickling, electropolishing, or electroplating. The maximum effect is usually observed near room temperature. This is where chemical activity and hydrogen mobility are high enough to produce and inject H into the material, but not so high as to promote its exit and loss by H_2 gas evolution. High pressure hydrogen gas or H_2S are other sources of a high hydrogen fugacity. Classic hydrogen embrittlement had first been associated with high strength ferritic (BCC) steels, but it has since been found in FCC stainless steels, Ni-base superalloys, and Al alloys, as well as a number of intermetallic compound phases.

A triaxial stress state favors the phenomenon. This provides a volumetric expansion, i.e., favorable sites attracting interstitial hydrogen, and diminished ability to blunt cracks via plastic deformation. Triaxiality exists ahead of an existing crack tip and provides a zone of hydrogen accumulation. Once a crack nucleates and begins to grow, it often arrests until additional hydrogen can diffuse ahead of the crack tip and provide a new embrittled zone. Thus, discontinuous subcritical crack growth is a common attribute. Accordingly, the phenomenon becomes apparent only at certain strain rates, low enough to allow hydrogen diffusion, but fast enough to prevent complete loss by recombination and gaseous escape.

Since preferential, short-circuit diffusion of hydrogen often applies, grain boundary fracture, though not necessary, is another frequent attribute. A negative synergy is often observed when other detrimental grain boundary segregants are present, such as S, P, or C. Furthermore, H-H recombination poisons in the environment, such as S and As, favor H injection (embrittlement) over innocuous escape as gaseous H_2.

The fundamental basis for hydrogen embrittlement is not fully resolved and remains an active topic of discussion. On one hand, ab initio studies have made a case for decreased M-M bond strength for H-contaminated interfaces. On the other, a mechanism supporting, paradoxically, enhanced local *plasticity*, describes 'embrittlement' and interfacial weakening due to a thin network of highly mobile dislocations. Embrittling metal hydrides and gaseous hydrogen bubbles have also been discussed as a root cause of embrittlement. For the present purpose of explaining moisture-induced scale spallation, any hydrogen embrittlement mechanism allowing for decreased interfacial strength is acceptable. The details of various possible, but still controversial, atomistic mechanisms are beyond the scope of this discussion.

Moisture-Induced Delayed Spallation (MIDS)

Proposed Mechanism

The elementary steps in the process are shown schematically in Figure 2. It can be postulated that local electrochemical cells develop at exposed oxide-metal interfaces in moist environments. Here H_2O is adsorbed on the exposed metal and dissociates to $(OH)^-$ and H^+. The amount of adsorption is a function of the relative humidity and has been discussed in regard to MIDS (Ref. 3) and will be addressed later. Anodic oxidation of aluminum from the alloy to Al^{+3} occurs at active exposed metal sites, resulting in $Al(OH)_3$ (or $Al_2O_3 \cdot nH_2O$). This frees e^- cathodically at protected (passivated) areas, attracting and reducing H^+. Hydrogen then diffuses interstitially under the scale. The biaxial tension, produced at the metal interface by CTE mismatch with the scale after cooling, provides an attraction for hydrogen.

Scale segments autocatalytically debond when the hydrogen concentration reaches a critical limit, reducing the interface toughness to where it can be overcome by the stored strain energy in the scale. This feature derives from the observation that scales directionally "unzip" as humid air is allowed localized access to an exposed interface. It is also proposed that the scale cracking and spallation process itself is near instantaneous (τ_{spall3}), previously requiring some finite time for water dissociation and hydrogen diffusion ($\tau_{incubate2}$), relegating the remaining scale to much longer residence times ($\tau_{intact1}$), or indefinite immunity as stresses are relieved adjacent to the numerous spallation sites.

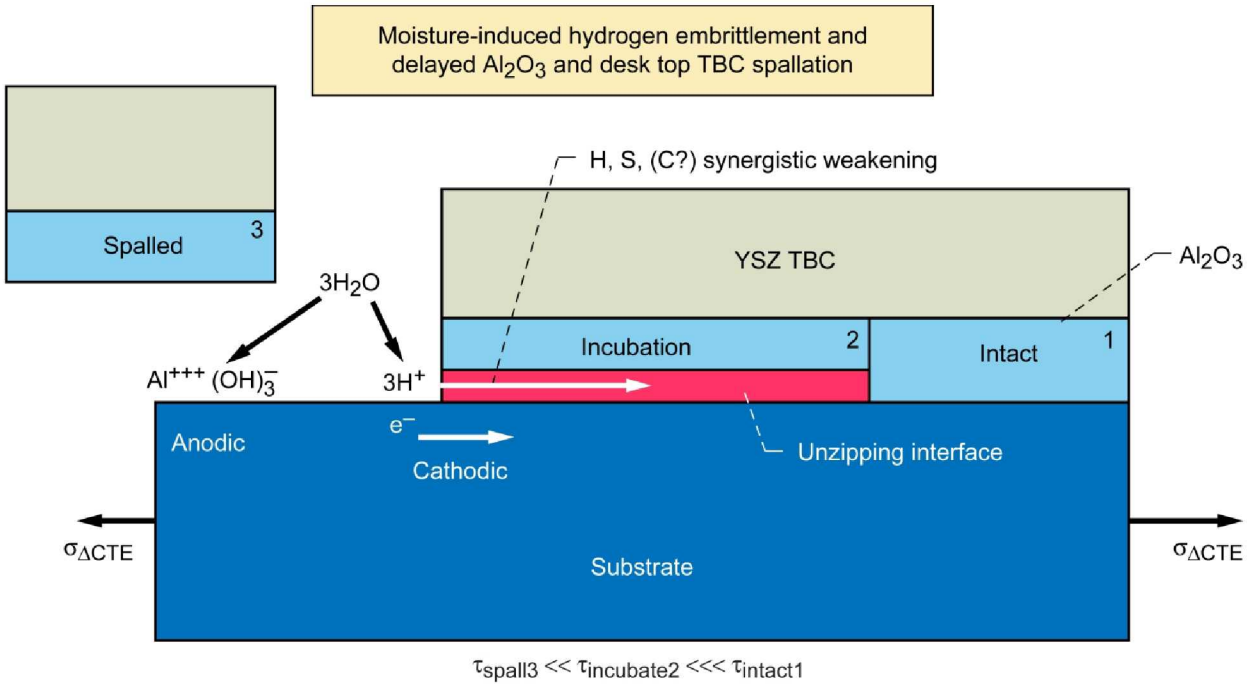

Figure 2.—Schematic of moisture-induced hydrogen embrittlement used to explain delayed spallation of alumina scales and desk top TBC spallation: a marginal Al_2O_3–metal interface, under high stress, is exposed to a moist environment; local electrochemical cells produce $(OH)^-$ to react with Al_{metal}, leaving H^+ to diffuse into the interface. With time, H diffusion progresses underneath the scale, further weakening the scale and allowing spallation to occur.

General Phenomenological Attributes

The early manifestations of this phenomenon were associated with a time factor after cooling from high temperature oxidation, i.e., after the sample was removed from a relatively low humidity (warm) furnace environment to more humid ambient conditions. Thus the term "delayed" is employed to distinguish from spalling immediately upon cool-down. This presumes of course that much of the scale must be retained initially, most likely excluding scales formed on undoped, relatively high sulfur (>10 ppmw) alloys. Samples given some propensity for spallation would be most susceptible to MIDS Typically this means a range and combination of prerequisite factors: undoped alloys, intermediate, ~1 to 5 ppmw, levels of sulfur, high strain energy (>5 to 10 μm thick), and cyclic damage exposing the scale-metal interface. This susceptibility is progressively decreased as sulfur is reduced below 1 ppmw, as Y, Hf, or Zr active element doping is employed, Pt additions made, or as high Al, e.g., Ni-50Al, compositions are used. For more adherent scales, a comparable degree of MIDS may take more cyclic damage, higher levels of humidity, higher levels of strain energy and longer time to be manifested.

Indeed a spectrum of MIDS behavior is seen as one or more of these factors are varied. It is helpful to view the phenomenon according to a spallation versus composition map that highlights a "sensitive zone" where MIDS may be most apparent, Figure 3. Using sulfur content as the major determinant of adhesion, a schematic representation can be constructed (taking cues from adhesion maps for PWA 1480 (Ref. 4)). Here, for moderate cyclic furnace oxidation exposures, a modicum of adhesion can be expected at ≤10 ppmw S and essentially full adhesion at ≤0.1 ppmw S, as approximated by the sigmoidal residual scale curve ***A*** after cooling:

$$\%\text{Area}_{\text{ret'nd}} = \frac{a}{e^{(b + c \log S)} + 1} \tag{1}$$

where S is the sulfur content in ppmw,
a is between 0 and 1,
b and *c* are constants, generally between 0 and 4.

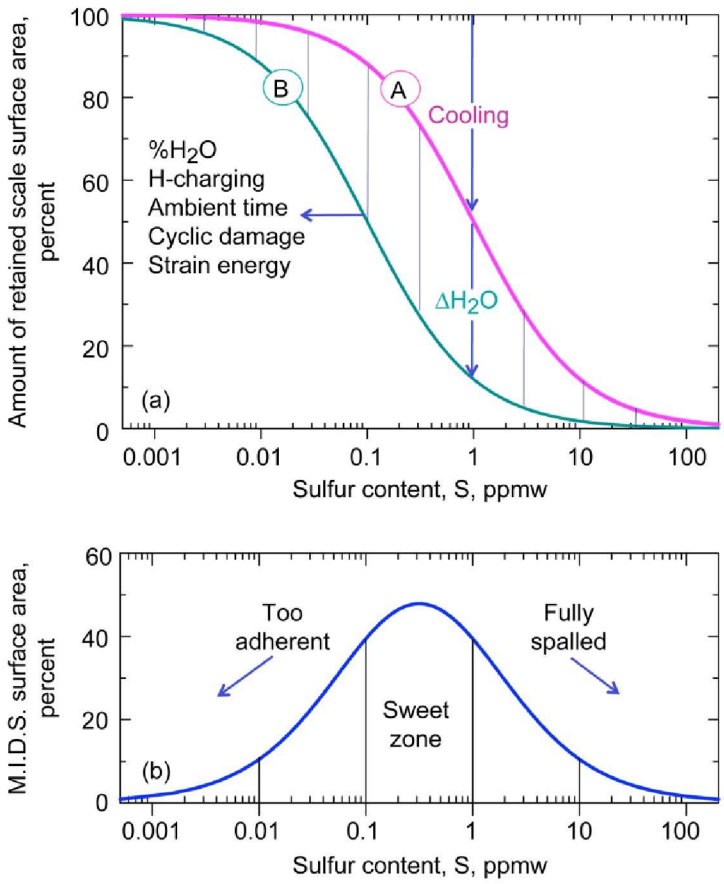

Figure 3.—Schematic of scale retention after cooling and subsequent exposure to moisture. (a) Total spallation occurs at high sulfur contents, transitioning to total adhesion at low sulfur contents. Curve A corresponds to surface after cooling, Curve B corresponds to surface after moisture induced spallation. (b) The amount of observable moisture induced spallation (Curve A – Curve B) is maximized as a "sensitive zone" having intermediate adhesion.

For $a = 1$, $b = 0$, and $c = 2$, we obtain the symmetrical sigmoidal curve shown in Figure 3(a), with an inflection point at 1 ppmw S and asymptotes at 0 percent retained scale for high S and 100 percent retained scale for low S. This locus can be shifted to the right (→), indicating higher adhesion at a given sulfur level, with reactive element dopants or Pt additions. Conversely, it can be shifted to less adhesion (←) if more strain energy is built up in the scale, i.e., with the scale thickness (oxidation time and temperature) and with the product, squared, of CTE mismatch times ΔT of cooling.

A second locus, curve *B*, can be constructed (using $b = 2$) to indicate the amount of retained scale following subsequent exposure to moisture. The amount of moisture-induced spallation is then represented as the cross-hatched region, shown in Figure 3(b) for curve *A* – curve *B*, or "sweet zone" for MIDS. Both ***A*** and ***B*** boundaries need to be considered to address the phenomenon: there may be too much initial spallation (before moisture exposure) to exhibit any additional spallation (band shifted left); or the adhesion may be so great and strain energy so low that no amount of moisture will trigger spallation (band shifted right). Curve *B* is also envisioned to shift to lower amounts of retained scale (←) and widen the sweet zone as the degree of additional moisture exposure, delay time, hydrogen charging, or amount of interfacial exposure (cyclic damage) increases. Residual interfacial stresses (tensile in the metal) may also be operative in attracting hydrogen into the interface and serve as an additive factor expanding this zone. Some specific examples will follow in the discussion of scale-metal interfacial failures, as in item III.C of the logic diagram outline, Figure 1.

I. Chemical Basis: H_2O Reacts With Al Powder to Produce H_2 Gas

In the discussions of moisture-induced hydrogen embrittlement of Al, Ni_3Al, Fe_3Al, and FeAl, it is often stated that water is chemically reduced by Al in the alloy to yield aluminum hydroxide (or aluminum oxide) and hydrogen according to Equation (2):

$$Al_{alloy} + 3H_2O_{ambient} = Al(OH)_3 + 3H_{ads} \quad (2a)$$

or:

$$2Al_{alloy} + 3H_2O_{ambient} = Al_2O_3 + 6H_{ads} \quad (2b)$$

At this point, it is not critical to specify whether the oxide or hydroxide forms. It is specified that atomic hydrogen is produced, which directly allows for adsorption onto and absorption into the alloy. If the hydrogen solubility is exceeded locally or if recombination exceeds solution and diffusion rates, H_2 gas may be evolved. Given the elusive nature of solved hydrogen and general difficulty of detection, H_2 gas evolution may offer an alternative means of verification by chemical analyses.

In that regard, we present the results of studies designed to evolve hydrogen gas by reacting Al powder in water (Refs. 5 to 7). Here, interestingly, the powder had to be modified to prevent instantaneous passivation and cessation of reaction. The authors pre-conditioned the powders by reacting (calcining) with substantial quantities of $Al(OH)_3$ at 600 °C. The result is a γ-Al_2O_3 –modified aluminum powder (GMAP), having apparent active sites on the metal preserved by contact with a stable, high diffusivity or porous oxide. Upon contact with liquid water, H_2 gas is evolved as measured by gas chromatography. For example, ~50 mole% of H_2, relative to the amount of Al metal present, was recorded for reacting with water at 50 °C for 7 hr, Figure 4 (Ref. 7).

These experiments with submerged Al powder represent an extreme compared to any reaction scheme between ambient moisture and an oxidized solid. For example, the degree of exposed metal is limited by the amount of scale cracking and spalling. The reaction should not occur for a completely intact healing scale. Secondly, the activity of Al in alloy solution would be orders of magnitude lower than that of pure Al. Finally, observed spallation events occur in ambient humidity, much less than the saturated vapor pressure of liquid water. These differences would likely reduce the overall reaction, and the small amounts of reaction product may escape detection by most conventional techniques.

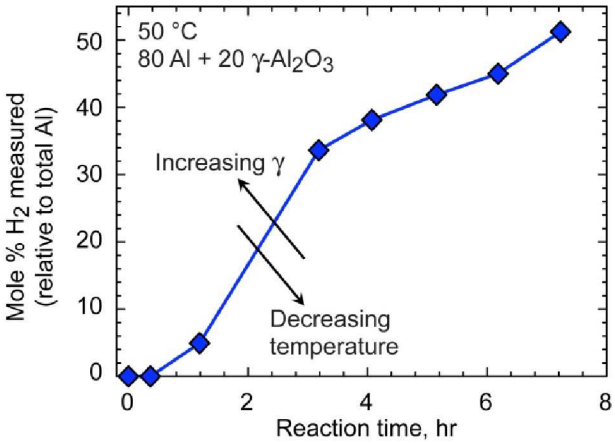

Figure 4.—Water-induced H_2 evolution from reaction with (γ-Al_2O_3-modified) Al powder, showing ~50 percent completion after 7 hr at 50 °C (Ref. 5).

Hydroxylation of alumina from adsorbed ambient moisture has also been discussed (Ref. 8). Here the pertinent reaction chemistry would be given by:

$$Al_2O_3 + 3H_2O_{ambient} = 2Al(OH)_3 \quad (3)$$

But here it is apparent that hydrogen is not produced by reaction (3), and any detrimental effects on interfacial integrity would depend on the much slower diffusion of molecular water along the interface.

Other supporting evidence is provided by a study of copper reactions with water at room temperature (Ref. 9). Here 0.3 mm thick copper sheet (140 cm^2) was exposed to low-oxygen content water in a closed vessel, with the vapor above the mix sealed by a palladium hydrogen permeability membrane. The other side of the membrane was high vacuum and connected to a mass spectrometer. It was found that H_2 gas was continuously generated over durations as long as 5000 hr. The explanation went as Equation 2(a), except that now the supposed metastable copper hydroxide reaction product was enabled only by the low oxygen content, with the adsorbed hydrogen of course combining and evolving as gaseous H_2.

II. Theoretical Justification: Al_2O_3-H-Metal Bond

Ab Initio Calculations

Given that exposed metal, containing reactive elements such as aluminum, will react with water and produce hydrogen as a by-product in some form, we then postulate that atomic hydrogen may enter the material by an adsorption/absorption sequence. Once at the interface, hydrogen may affect the strength of scale-metal adhesion. There is a growing body of work addressing the theoretical strength of alumina-metal interfaces and the effects of impurities and dopants, through quantum chemical models and ab initio calculations. In general, sulfur has been found to significantly weaken the interface, in agreement with experimental findings (Refs. 10 to 13). Reactive element dopants strengthen the interface while simultaneously binding sulfur and preventing mobility.

Interstitials, such as carbon and hydrogen, are not as widely studied, but the work of Smith et al. is relevant to the present case (Refs. 14 to 17). In that regard we cite his ab initio density functional theory (DFT) study of C and H levels at the (0001) α-Al_2O_3 interface with 1/3 monolayers of (111) Co and Cu films. Here the lowest energy interstitial structure is determined over a range of C and H chemical potentials, producing the equivalent of a 2-D phase diagram for C and H surface atoms. It was found that 6 distinct structures resulted with specific C, H concentrations residing within a 2-oxygen atom surface cell. Next the work of adhesion for Co and Cu films is calculated for each stable configuration.

For purpose of illustration, the calculated values are displayed for each structure according to the alumina surface structure C-H composition in Figure 5. Actual data points corresponding to six stable structures are shown as the stars. (The 3-D mesh response surface is a conservative interpolation. It is displayed only for the purpose of illustrating overall trends, since some of the grid points apply to unstable structures.) For the most part, it is seen that increasing H content results in a decrease in interface adhesion, for example, by as much as 90 percent in going from the 0H-3C structure to 3H-3C.

A similar trend is observed for Cu-Al_2O_3 interfaces, Figure 6, except that the overall magnitudes are about 1/2 those of Co-Al_2O_3. Furthermore, an analogous study by Smith et al., (Ref. 15) calculates the work of separation to decrease from 7.02 to 4.72 to 0.63 J/m^2 for clean, 1/3 ML, and 1 ML (monolayer), respectively, of interfacial hydrogen. Here 1 monolayer is defined as 1 H atom for every surface O atom.

Some limitations are acknowledged. There was no calculation for strictly hydrogen effects without carbon in Figures 4 and 5; i.e., the clean interface value was determined only for the stable clean Al terminated α-Al_2O_3, while the C-H interface values were determined for O-terminated α-Al_2O_3 for the stable H-modified surface. For the specific case of alumina scales, the high Al activity corresponding to the low pO_2 of the interface results in an Al_2-terminated oxide. So the trends shown in Figures 5 and 6 must be implicated for that more appropriate type of surface (Ref. 17).

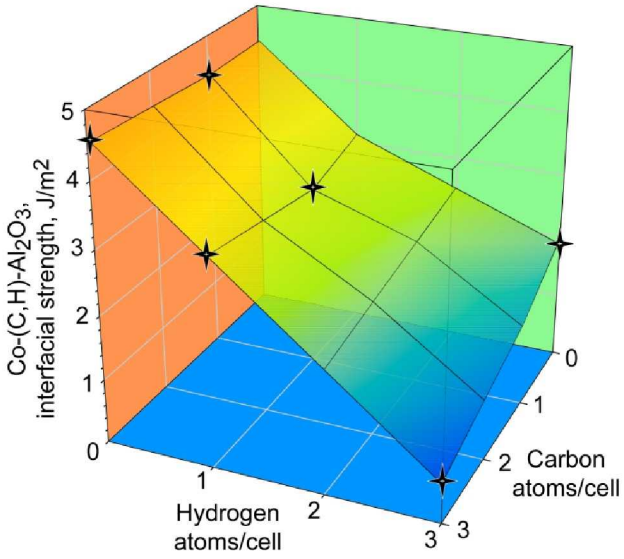

Figure 5.—Ab-initio prediction of hydrogen-induced Co-Al_2O_3 interfacial weakening (symbols for 2-D stable arrangements). Interpolation/extrapolation surface of DFT calculations (Ref. 16).

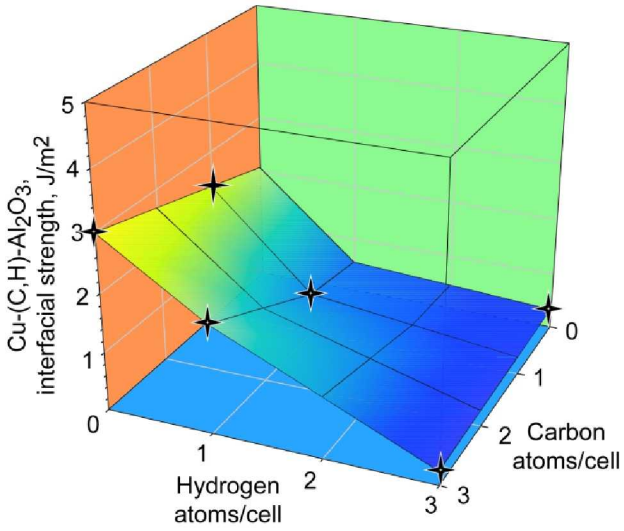

Figure 6.—Ab-initio prediction of hydrogen-induced Cu-Al_2O_3 interfacial weakening (symbols for 2-D stable arrangements). Interpolation/extrapolation surface of DFT calculations (Ref. 16).

TABLE 1.—EFFECT OF MOISTURE ON Ni(Cr)-Al_2O_3 INTERFACIAL FRACTURE TOUGHNESS (REFS. 19 TO 22)

Metal	Oxide	Atmosphere	Segregant	J/m^2 toughness	References
Ni	Al_2O_3	Dry N_2	C	>100	Ref. 19
Ni	Al_2O_3	Air[a]	C	10	
Ni20Cr	Al_2O_3	Air[a], dry N_2	C, no S	>100 to 300	Ref. 20
Ni20Cr	Al_2O_3	Air[a]	C, S[b]	2 to 7	
NiAl	Al_2O_3[c]	Air[a]	yes	5	Ref. 21
Ni	Al_2O_3	oil	0.19[d]	34.2	Ref. 22
Ni	Al_2O_3	air	0.19	19	
Ni	Al_2O_3	air	0.45	17.7	
Ni	Al_2O_3	air	0.55	8.5	

[a]50 percent relative humidity at 20 °C
[b]~3 percent at surface
[c]TGO, 1 to 100 hr at 1000°, 1100 °C
[d]S/Ni AES ratio

Double Beam Interfacial Toughness, Ni-X-Al_2O_3

A negative effect of moisture on alumina-metal interface strength has been demonstrated by the fracture mechanics studies of Evans et al. and others. These generally entail diffusion-bonded sandwiches of polished sapphire plates and ultra-pure metals and alloys. Compression or bend bars were machined from the sandwiches, and exposed to a pre-drilled interface hole or pre-cracked by an overloaded Knoop microhardness indentation. The interface toughness was then resolved from the resulting crack growth behavior through classic K_{IC} relationships, as summarized in (Ref. 18), reconstructed here as Table I.

In the first study (Ref. 19), the effect of ambient air was determined for the toughness of Ni-Al_2O_3 interfaces. First, in dry N_2 environments the interface toughness could only be estimated as >100 J/m^2 because the crack did not run along the interface. However, it did follow the interface and was reduced to 10 J/m^2 when measured in ambient (50 percent relative humidity) air. Carbon was a known interfacial impurity and behaved synergistically with moisture.

The toughness of Ni20Cr-Al_2O_3 interfaces was insensitive to ambient air because of the gettering effect of Cr and the stability of Cr-carbides (Ref. 20). Again, the failure did not run along the interface so the toughness lower bound could only be estimated as >300 J/m^2. However, when the composite was exposed to a 'liquid' phase anneal, above the melting point of any CrS precipitates, the interface failed in ambient air from residual thermal expansion mismatch stress, without the need for any external stress. Now the interface was contaminated with S and C. A toughness range of 2 to 7 J/m^2 could only be estimated. This data for Ni20Cr-Al_2O_3 emphasizes the negative synergy between moisture and sulfur. In a sense it fortells the "sweet zone" where moisture effects on scale spallation are maximized for interfaces that are partially compromised by some segregation and high strain energy.

A subsequent study examined the scale formed on a NiAl – coated superalloy (Ref. 21). From scale buckling measurements versus applied compressive stresses, it was surmised that stable buckle delamination propagated with an interface toughness of only ~5 J/m^2 in moist air. The alloy contained no reactive element dopants, and therefore the segregation of impurities was presumed.

Finally, the deformation of double-cleavage, drilled compression samples was evaluated in two environments at various sulfur segregation levels (Ref. 22). It was found that ambient humidity at a given sulfur content decreased the interface toughness from that measured under water-free oil, as did further increases in the sulfur interface concentration.

The above experiments indicate the negative effect of moisture on bulk interfacial Ni-Al_2O_3 adhesion. Negative synergy between moisture, S, and C are indicated. However, it remains to be shown that hydrogen, according to the present mechanism, is created for less reactive Ni and NiCr alloys if there is no aluminum to react with moisture according to Equation (2).

III. Interfacial Failures:

III.A. Bulk Nickel Aluminides (And Related Alloys)

A great deal of interest had been generated for potential high-temperature, low-density, oxidation-resistant structural aluminides, specifically NiAl, Ni_3Al, FeAl, and Fe_3Al. In the case of β-NiAl, room temperature ductility has still not progressed to conventional values, no matter what alloying schemes were adopted to maximize strength and no matter what testing conditions were adopted. In other words an intrinsically brittle material remained brittle. However in the case of the other aluminides, single crystals, microalloying, test conditions, and test environment had profound effects on room temperature ductility. The question of intrinsic and extrinsic grain boundary embrittlement became an issue, eventually reaching the atomic level of dislocation type and mobility. For a time, extrinsic embrittlement was simply precluded by ductility-enhancing B and Zr additions, until the true environmental effect was revealed. All the pertinent aspects of moisture-induced embrittlement of aluminides have been expertly reviewed by key researchers, (Stoloff, Duquette, Liu, Chen) and form the basis of the summary below (Refs. 23 to 26).

The enigmatic behavior of so-called brittle intermetallics was finally resolved by early studies of FeAl and Fe_3Al that included a comparison of low tensile ductility measured under ambient conditions with higher values determined under vacuum or dry O_2 (Refs. 27 and 28). The results implicated ambient moisture (relative humidity) as the source of hydrogen, a notorious embrittling agent. It was already clear that cathodic hydrogen charging embrittled even the intrinsically ductile Ni_3Al+B,Zr alloys (Refs. 29 and 30). The broad spectrum of environmental effects can be seen by the telling nature of the stress strain curves obtained under different conditions, as shown in Figure 7 (Ref. 23). Here the degree of plastic deformation in a tensile test can be seen to increase on a stress strain plot according to the decrease in hydrogen in the material or hydrogen or moisture in the test environment. The telling broad spectrum, ranging from 1 to 13 percent ductility, can be seen to vary from in-situ continuous electrochemical hydrogen charging, pre-charging only, H_2 gas, moist air, dry air, to dry oxygen. Similar effects are presented for FeAl and Fe_3Al, Figure 8, where the overall embrittling trend follows vacuum, dry O_2, ambient air, 4%H_2/Ar, and H_2O vapor, with an anomalous effect for FeAl in vacuum (Refs. 27, 28, and 33).

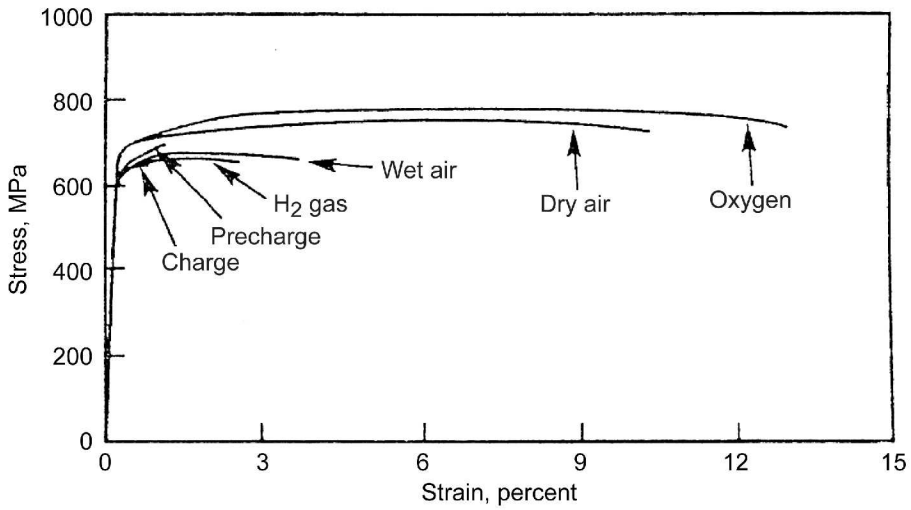

Figure 7.—The embrittlement effects of hydrogen and moisture in tensile stress/strain behavior of Fe_3Al; strain rate = 3×10^{-6}/s (used with permission from Ref. 23).

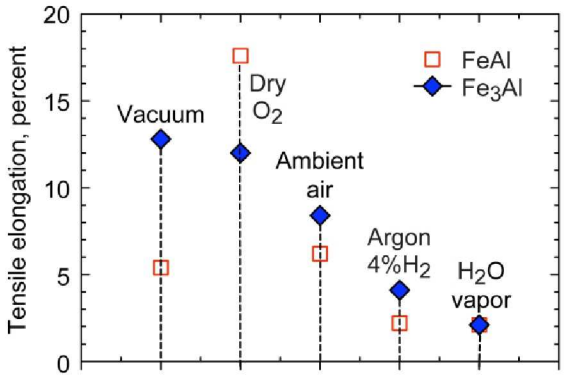

Figure 8.—Reduced tensile ductility of FeAl and Fe_3Al due to moisture and H_2 (Refs. 27, 28, and 33).

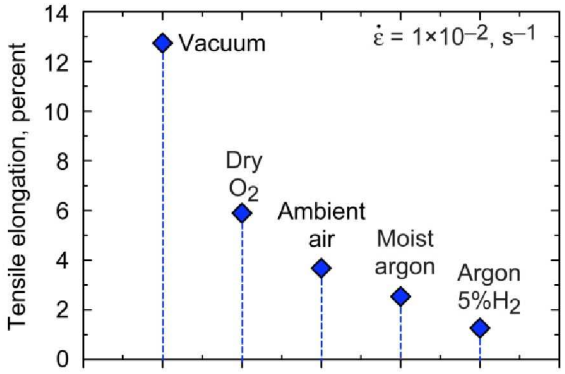

Figure 9.—Reduced tensile ductility of Ni_3Al due to moisture and H_2; strain rate = 1×10^{-2}/s (Refs. 31 to 33).

Since hydrogen diffusion is involved, a time factor becomes apparent. In the case of tensile testing, strain rate dependence of embrittlement is often observed. Thus the above data was obtained at a constant strain rate of 3×10^{-6}/s, generally low enough to allow any potential embrittlement to occur. Other data for Ni_3Al, obtained at or interpolated to 10^{-2}/s from (Ref. 26), is shown in Figure 9. Here the ductility trend increases from 5%H_2/Ar, moist Ar, moist air, dry O_2, and vacuum (Refs. 31 to 33). Another set of data varied the total pressure, but clearly related embrittlement to the effective p(H_2O), Figure 10. Here the ductility is seen to steadily decrease with p(H_2O) increasing from UHV (~10^{-9} Pa) to ambient conditions (~10^3 Pa). (Refs. 31, 32 in 26).

Other Alloy Studies

Analogous moisture-induced phenomena have been studied for conventional Ni-base superalloys under the mantle of *gas-phase embrittlement*. A pertinent example is the recent study of alloy 718PLUS by Hayes (Ref. 34), which highlights the progression of intergranular embrittlement in V-notch tensile tests over the temperature range of 704 to 871 °C. Initial hold times of ~1 to 2 hr in bottled air, lab air, and humid air were used to allow various degrees of interdiffusion and environmental embrittlement. The latter depth was evaluated from optical macrographs of the outer intergranular zone of the fracture surface. The results for the embrittlement kinetics at 704 °C and the activation energy over the

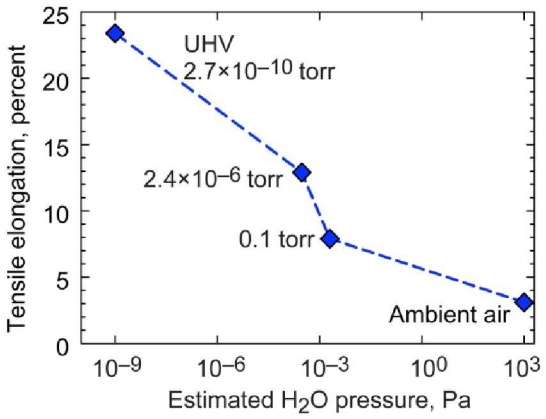

Figure 10.—Reduced tensile ductility of Ni_3Al due to $P(H_2O)$ estimated from total pressure (Refs. 26, 31, and 32).

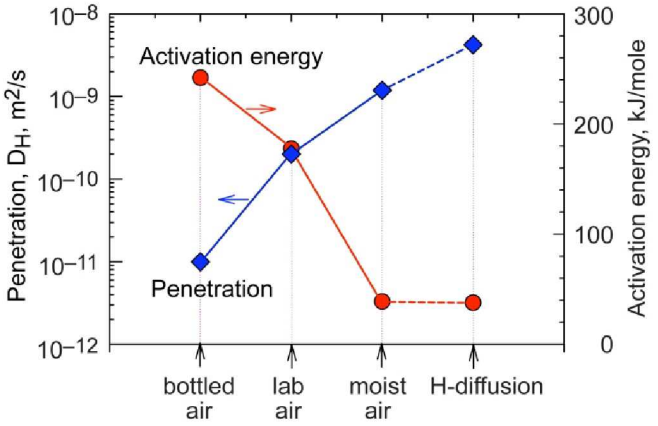

Figure 11.—Embrittled zone penetration kinetics of alloy 718PLUS V-notch tensile tests in various environments, 704 °C (Ref. 34). Penetration kinetics and activation energy approach those for hydrogen diffusion in Ni.

temperature range studied are re-constructed in Figure 11. Here it is seen that the kinetic factor of embrittlement increases with the degree of moisture in the atmosphere, though some baseline oxygen embrittlement is certainly observed in the dry bottled air as well.

The kinetics are compared to those measured for hydrogen diffusion in pure Ni (Ref. 35) and show some convergence with increasing humidity (dashed line). The activation energies for the embrittlement zones were also determined and are summarized on the same plot. Here it is seen that the activation energy decreases with increasing levels of moisture, now converging exactly on the value measured for diffusion of hydrogen in Ni. Hayes discussed these results in the context of a wide body of relevant literature and concludes that gas-phase embrittlement is controlled by diffusion into the alloy. Moist environments may result in rapid hydrogen diffusion and more severe embrittlement, with the gradation in attack severity increasing from oxygen to hydrogen control.

This brings us to the general phenomenon of grain boundary hydrogen embrittlement of Ni, fundamental to the previous discussions of moisture effects. Much has been established in the elegant, basic work of Birnbaum et al. For example, in (Ref. 35) cathodic hydrogen experiments produced grain boundary embrittlement in 77 K tensile tests. Embrittlement occurred for current densities above 0.4 mA/cm^2 in an $NaAsO_2$ - poisoned 1N H_2SO_4 solution. The 77 K tensile ductility (fracture strain) was reduced from 30 to 3 percent by cathodic hydrogen charging at 500 A/m^2 for 80 min at 314 K. A rim of brittle grain boundary fracture was apparent from fractographs, progressing inward with charging time. The critical hydrogen grain boundary content to produce embrittlement was found to be H/Ni = 0.065. Diffusional analyses established the following relation for hydrogen grain boundary diffusion (Eq. 4a), yielding 8.0×10^{-14} m^2/s, approximately 2× the value for lattice diffusion, 4.5×10^{-14} m^2/s (Eq. 4b) near room temperature:

$$D_{GB}^{H} = 4.4\times10^{-7}\left(\mathrm{m^2/s}\right)\exp\left(\frac{-37.8\,\mathrm{kJ/mol}}{RT}\right) \tag{4a}$$

$$D_{L}^{H} = 4.8\times10^{-7}\left(\mathrm{m^2/s}\right)\exp\left(\frac{-39.4\,\mathrm{kJ/mol}}{RT}\right) \tag{4b}$$

Furthermore, doping with sulfur (104 ppma) enhanced the sensitivity to hydrogen embrittlement, showing more embrittlement at shorter charging times and lower current densities, while carbon (220 ppma) decreased this sensitivity. At one extreme, annealed and quenched Ni-S material was ductile until cathodically hydrogen charged. At the other extreme, the critical level of H/Ni for embrittlement was reduced by the presence of sulfur segregated at the grain boundaries.

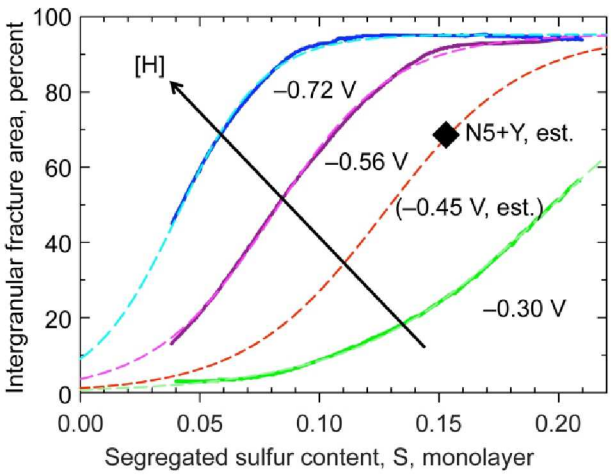

Figure 12.—Grain boundary embrittlement of Ni due cathodic hydrogen charging (Ref. 36). Idealized sigmoidal curves for various potentials, measured against a saturated calomel electrode, and corresponding curve fits (dashed). Interpolated (dashed red) curve at the cathodic descaling potential used on René N5 (Ref. 2) and estimated maximum interfacial sulfur (diamond) from surface recession, (Ref. 74).

This synergistic, or at least additive, effect of sulfur and hydrogen on interfacial embrittlement is a recurring theme. For example, similar conclusions were reached by Jones et al. in studies of cathodic hydrogen embrittlement of Ni as a function of grain-boundary sulfur segregation, (measured by Auger), and cathodic potential (measured against a saturated calomel reference electrode) (Ref. 36). In Figure 12 it is shown that brittle intergranular fracture increased sigmoidally from ~2 to 95 percent as the S/Ni segregation level increased from 0.04 to 0.20 and as the negative (cathodic hydrogen charging) potential increased from –0.30 to –0.56 to –0.72 V. (These curves are shown as idealized curves from (Ref. 36) along with sigmoidal curve fits (dashed), producing R^2 values >0.99. An interpolated curve at –0.45 V is also produced, and will be discussed later in regards to cathodic descaling at this potential). The sigmoidal response with sulfur content and the reinforcing interaction of interfacial S and H shown here are also strongly implied in the moisture-induced spallation data as a function of sulfur content, similar to the sensitivity zone model and in the spallation data discussed later (in III.C Alumina Scales – sulfur dependence, Figure 19).

Hydrogen Detected in Aluminides

Chen and Liu (Ref. 26) site a few studies indicating that hydrogen is produced by reaction of water with aluminides, e.g., time-of-flight (ToF) mass spectrometry showed a 4 to 20x increase in hydrogen for water- treated Fe-36Al. Similarly, a temperature programmed desorption experiment with deuterium oxide (D_2O)-treated $Ni_3(Al,Ti)$ revealed a D_2 peak at 350 K, without any corresponding D_2O background peak. Here the implication is that the heavy water treatment did result in absorbed D_2 from reaction with the alloy.

Supporting Critical Experiments

The demonstrations of embrittlement in H_2–containing atmospheres or by cathodic hydrogen charging are strong evidence that the key factor in moisture induced embrittlement of aluminides is *hydrogen*. What can be taken from the studies of bulk aluminides is that any environmental source of moisture is a potential source of hydrogen and environmental (extrinsic) embrittlement. Thus various related phenomenon come in to play depending on the specific test environment (strain rate, test temperature, adsorbed moisture, hydrogen dissociation, other grain boundary segregants), and the same framework can then be applied toward understanding MIDS.

III.B. Anodic Films on Aluminum

Another compelling analogy to moisture induced alumina scale spallation is presented by the thin films formed on aluminum and aluminum alloys. Moisture has been found to compromise thin native-oxide films or those formed anodically or by electropolishing. Decohesion and loss of protection has been observed. In the extreme, hydrogen embrittlement of the alloy may result. Many of these features have been pointed out in the works of Scamans et al., and Shimizu, Skeldon, Thompson et al. (Refs. 37 to 41). The initial film is an amorphous alumina based on γ-Al_2O_3. Subsequent exposure to moisture involves the basic chemistry similar to that put forth for the aluminide situation. Now boehmite (and pseudo-boehmite), AlOOH ($\cdot$ xH_2O) are observed in addition to $Al(OH)_3$ bayerite. But both reactions produce 3H atoms for every Al atom reacted, just as shown in reaction 2a,b above, enabling various hydrogen-induced phenomena (Ref. 38).

A telling experiment involved the exposure of electropolished Al and Al alloys to 100 percent relative humidity (saturated) air at 70 °C. Bubbles, blistering, and scale-metal decohesion took place depending on the alloy and length of exposure, as long as condensed moisture was enabled. Nucleation of hydrogen bubbles at grain boundaries in sensitized alloys and dislocations was observed by TEM (Refs. 37 and 38). An example of 5 μm bubbles formed in the film is shown in Figure 13. Here the native oxide was allowed to form by exposure to room air for 24 hr., followed by exposure to 70 °C saturated air, inducing blisters of films on pure Al and Al alloys within minutes.

H Detected Under Alumina Films

In general, the detection of hydrogen requires some specialized techniques. In the case of thin films on Al, moisture exposures have been characterized by glow discharge optical emission spectroscopy (GDOES). By depth profiling, hydrogen as well as various other aqueous impurities or alloy constituents may be identified in the film. For Al electropolished in CrO_3-H_3PO_4, GDOES has been used to obtain chemical profiles, showing H, Al, Cu, P, and Cr distributions. It was stated that "…the surface film is hydrated across its thickness….the hydrogen profile exhibits two maxima at regions close to the surface and film-metal interface" (Ref. 39). Other studies characterized films produced by a wide variety of electrolytes (Ref. 40). Here hydrogen distributions (and W, Mo, B, P, Si) were documented for films produced in sodium tungstate, ammonium penta-borate, sodium chromate, potassium permanganate, ammonium dihydrogen phosphate, and ammonium citrate electrolytes. In every case, a discernable H peak has been observed at the film-metal interface. Again this indicates a propensity for hydrogen released from the reaction of Al with moisture to segregate at the alumina-metal interface.

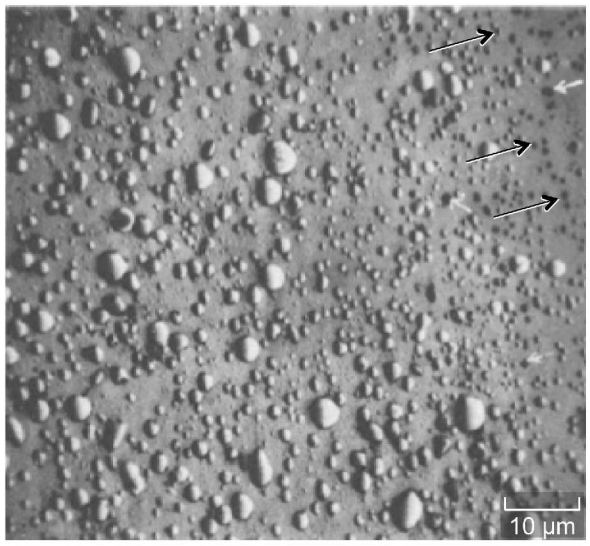

Figure 13.—Moisture induced blisters in native alumina film on aluminum caused by exposure to water vapor saturated at 70 °C (used with permission from Ref. 38).

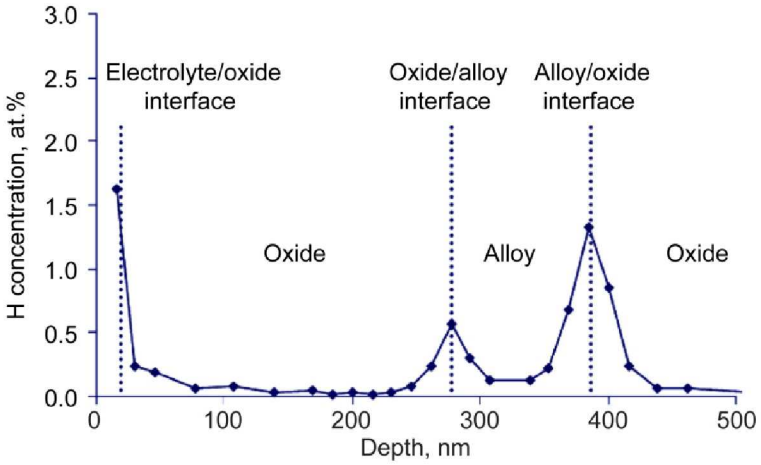

Figure 14.—Preferential hydrogen segregation at anodic oxide-aluminum metal interfaces by nuclear reaction analyses. Pre-anodized in 0.1 M Na_2WO_4 at 20 °C (used with permission from Ref. 41).

Nuclear reaction analyses (NRA), coupled with a high energy ^{15}N beam from an accelerator, was also used to characterize 200 to 250 nm anodic films grown on an Al-6.5 at.% W alloy in 0.1 M sodium tungstate (Ref. 41). Distinct H enrichments were found at the film-alloy interface, in accord with the observations above. Enrichments on the order of 1.5 at.% H were proposed, as shown in Figure 14.

One final note added in proof is the GDOES profile of a *chromia* scale formed on SUS 430 stainless steel at 900 °C after 6 hr. exposure to N_2-2.4%O_2-19.7%H_2O (Ref. 42). Here, again, a slight enrichment of hydrogen was detected at the vicinity of the scale-metal interface. Thus general support is given to the phenomenon of hydrogen segregation at scale-metal interfaces in the presence of moisture.

Supporting Critical Experiments

Strong support that hydrogen is the basis for moisture induced delamination of thin films is offered by the following study of externally applied hydrogen (Ref. 43). Here ion implantation of H^+ was performed on electropolished pure Al, anodized to produce films from 3 to 14 nm thick. After ion implantation with 100 keV H^+, at a fluence of 5×10^{13} ions/cm^{2}s and total dose of 6.6×10^{16} ions/cm^2, the films were noted to blister and peel off. It was further calculated that both implanted 10^{14} H^+ and 10^{15} aluminum vacancies were created in the near surface metal area. Thus it could be theorized that either or both H^+ and Al interfacial vacancies may be responsible for film decohesion.

For this reason, subsequent experiments utilized H^+, D^+, and $^3He^+$ ion implantation at comparable fluxes (Ref. 44). They found similar blistering and delamination for 60 to 110 keV H^+ and D^+ ions. An example of such delamination by H^+ implantation is shown in Figure 15 for a 120 nm film. The circular features are indicative of individual blisters, while the large sheet is a continuous delamination of the film. Since the He^+ ions have up to 4x the mass of the hydrogen ions, they would be expected to produce many more vacancies. However no film deterioration was found for $^3He^+$ or $^4He^+$, even up to 270 keV. It was therefore concluded that the smaller hydrogen atom was the key to separation, not vacancy coalescence or He species. That is, the higher mobility of H compared to He near room temperature allows for accumulation of a hydrogen species at the oxide-metal interface. Furthermore, they identified a minimum dose of ~3×10^{15} ions/cm^2, below which delamination does not occur, whereas extensive delamination did occur for 3×10^{16} ions/cm^2. Similarly, 60° off-angle irradiation, resulting in only partial penetration of a 500 nm film, produced no damage, whereas at 90° normal incidence, which penetrates the film, did result in blister formation.

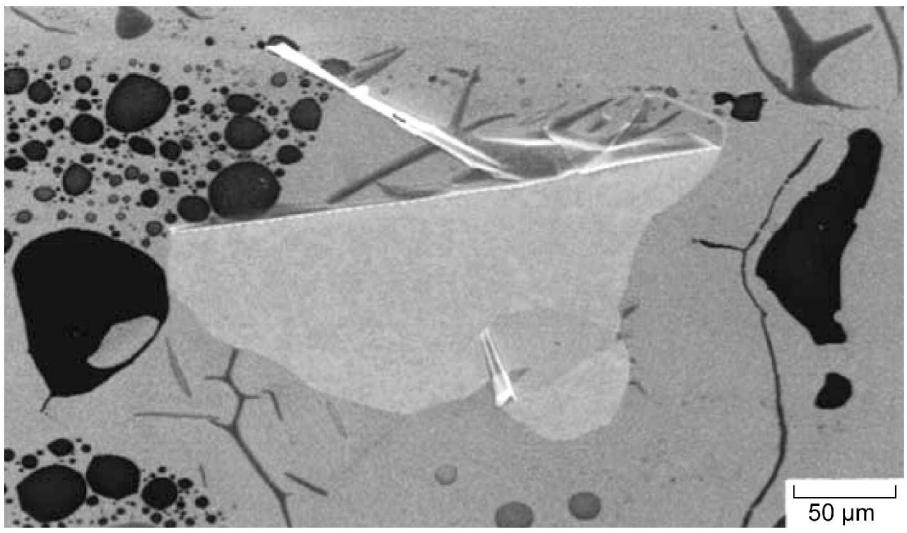

Figure 15.—H-implantation induced bubbles and blister failure of an anodic alumina film on aluminum. FEG-SEM micrograph of 120 nm film, 110 keV D+ ions, 1×10^{17} ions/cm^2 (used with permission from Ref. 44).

III.C. Alumina Scales

This finally brings us to the problem at hand, namely, moisture effects on alumina scale spallation. The experimental evidence for moisture-induced delayed spallation spans two decades and many research groups. Recent reviews of our experience and various corroborating studies have summarized most instances of MIDS and the related desk top spallation (DTS) phenomenon for thermal barrier coatings (TBC's) (Ref. 45). The first dramatic exhibition, perhaps, occurred for scale stripping by water immersion of sulfur-purged NiCrAl (Ref. 46). Subsequently, moisture phenomena have been documented for FeCrAl-X, PWA 1480, PWA 1484, René 142, René N5, René N6, plasma sprayed and physical vapor-deposited (PVD) TBC's, plasma-sprayed NiCoCrAlY and vapor deposited Ni(Pt)Al aluminide bond coats, and no bond coat, plasma-sprayed TBC systems (Refs. 3, 47 to 64).

Time Delay

While the immersion test often produces immediate results, it is perhaps more problematic to document the natural delayed spallation process in ambient humidity. The latter is of practical significance since reproducibility problems may arise for typical cyclic-oxidation testing due to uncontrolled test and measurement procedures. Addressing that issue, a time delayed spallation curve is presented for a commercial Ni(Pt)Al coating on CMSX4, oxidized at 1150 °C for up to 2000 1-hr cycles Figure 16 (Ref. 3). It can be seen that continuous spallation, though slight, occurred well after cool-down, for perhaps as long as 24 hr. It should be pointed out that this MIDS effect was correlated with prior surface rumpling at coating grain boundaries. Also, the overall behavior was still quite protective, exhibiting only a 3 mg/cm^2 weight loss after 2000 cycles (Ref. 3). Less adherent scales would be expected to exhibit more rapid and extensive MIDS response, according to the schematic "sweet zone" in Figure 3. Conversely, more adherent systems would be expected to show less MIDS. This was demonstrated for a duplicate sample, with clearly reduced grain boundary rumpling, where essentially no MIDS was measured in exactly the same test as Figure 16 (Ref. 3).

The physio-chemical mechanisms operating in ambient humidity for the typical cyclic tests shown above would be expected to be triggered by adsorption of moisture. Thus Equation (2) can be more precisely written as:

$$Al_{alloy} + 3(H_2O)_{ads} = Al(OH)_3 + 3H^+ + 3e^- \quad (5)$$

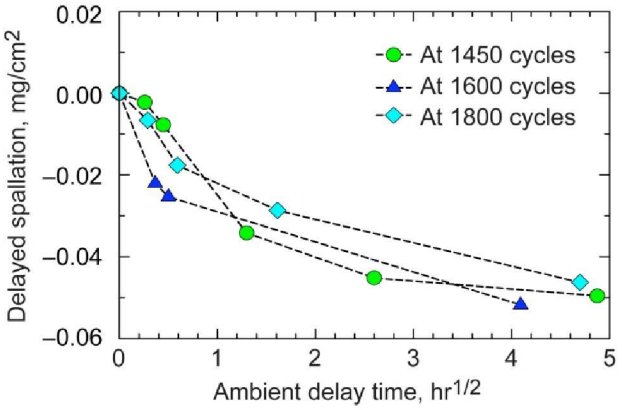

Figure 16.—Delayed alumina scale spallation after cycling Ni(Pt)Al-coated CMSX4 at 1150 °C. Weight change and time after initial measurement in ambient air, 1-hr cycles (Ref. 3).

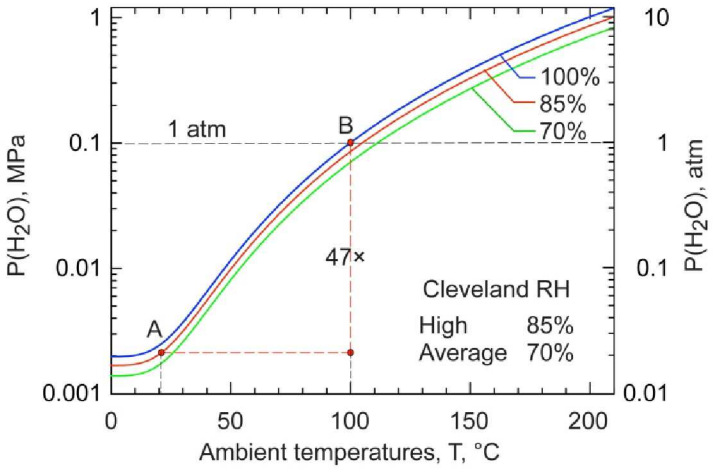

Figure 17.—Temperature dependence of water vapor pressures at saturation and typical relative humidity levels. Saturation values and moisture contents at the ambient balance conditions (A) compared to saturation values for the cooling chamber (B). A relative humidity of 85 percent at ambient temperature translates to 2.1 percent RH at 100 °C (Ref. 3).

Adsorption has been discussed as a function of the relative humidity (RH) and its increase by transferring samples from a warm (100 °C) furnace environment to the ambient laboratory condition (20 °C) (Ref. 3). The moisture content of air is shown as a function of temperature and typical relative humidity in Figure 17. At 100 percent RH, the corresponding saturated moisture content is seen to decrease substantially by reducing the temperature. One determines that the relative humidity in the 100 °C cooling chamber is only 2.1 percent. Consequently, removing a sample from the cooling chamber to the ambient at 85 percent R.H. essentially exposes the sample to a 40x increase in relative humidity (Ref. 3).

Furthermore, it has been shown that, in general, the amount of adsorbed water on metal surfaces is indeed directly related to RH, such that ~0.1 monolayer can be expected for RH = 2 percent and ~5 to 10 monolayers for RH = 80 percent (Ref. 65). That is to say, the amount (monolayers) of adsorbed moisture would be predicted to increase 50 to 100x upon removing the sample from the furnace cooling chamber. Thus a commensurate increase in $[H]^+$ is predicted according to Equation (4), along with a corresponding decrease on interfacial strength.

MIDS is correspondingly enhanced with extreme moisture exposure, as in water immersion. Accordingly, acoustic emission can be used during immersion tests to reveal extended time delays in spallation events. In one study, samples of René N5 with various Y levels were oxidized at 1150 °C for up to 1000 1-hr cycles. After cool-down, the samples were immersed in room temperature water and monitored by acoustic emission (Ref. 55). The response of three samples, with nominal sulfur levels of 5 ppmw and nominal cast Y levels of 88, 103, and 105 ppmw is shown in Figure 18(a). Note the intermittent rapid nature of the response, but spread over a period of ~24 hr. In contrast, hydrogen annealed samples revealed minimal activity, Figure 18(b). (The acoustic emission data for scale spallation was substantiated by the additional weight losses, number of spall segments, and spalled area due to immersion) (Refs. 45, 53, and 55). Since these samples were Y-doped, desulfurization did not occur. The improved adhesion was possibly due to decarburization, from ~500 to 100 ppmw C. Any detrimental effect of carbon may be associated with a slight downward trend in ab initio predictions for work of adhesion, Figure 5. However, it should be noted that carbon is also associated with decreased hydrogen grain boundary embrittlement in Ni (Ref. 35).

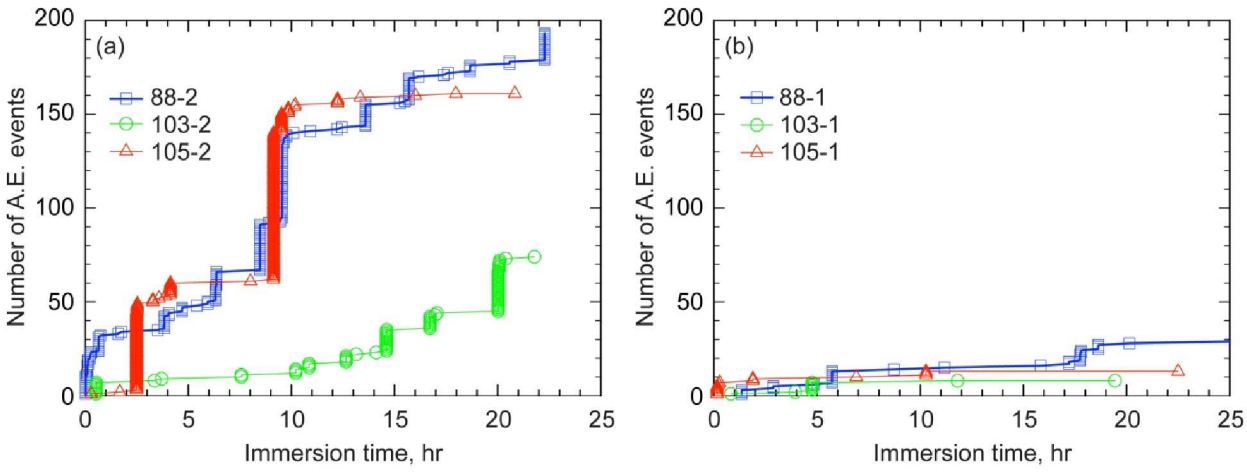

Figure 18.—René N5+Y oxidized at 1150 °C for 1000 1-hr cycles. (a) Delayed spallation detected by acoustic emission during water immersion. (b) Minimal delayed spallation during water immersion (hydrogen annealed at 1250 °C for 100 hr prior to oxidation) (Ref. 55).

Alloying/Impurity Effects on Adsorption/Absorption

Implicit in the initial steps of any hydrogen absorption process, various surface catalytic steps may be envisioned. In broadest terms, H must be adsorbed during the breakdown of the water molecule, but subsequent recombination (and desorption loss as H_2 gas evolution) must also be prevented. Accordingly, a number of catalytic alloying effects on Pt, Fe, Ni, Ta, and Ti substrates may be pertinent, as reviewed in (Ref. 66). These studies use hydrogen permeation, ductility loss, and H-sputter profiles to monitor H-absorption for exposures to hydrogen-containing environments (NaOH, H_2SO_4, HCl, and H_2). Pt, being an excellent catalyst, reduced hydrogen absorption for Fe and Ta. Ti, Y, and O, serving as H-active getters, increase absorption in Fe and Ni, but then trap hydrogen in stable complexes. Sulfur, a well-known poison for H-recombination as H_2 on Pt catalysts, would be expected to encourage H absorption. Indeed, sulfur site competition and decreased H sticking coefficients on S/Pt and S/Ni contribute to reduced surface stability of H and decreased recombination efficiency. Thus, sulfur can be viewed as a facilitator of H incorporation, while Pt, Ti, and Y can be viewed as reducing H effects, in line with existing trends for scale adhesion.

Sulfur Dependence

Desulfurization studies of PWA 1480 (by annealing in 5%H_2-Ar) provided a convenient process for removing sulfur in a controlled fashion (Ref. 67) according to the diffusion product, $4D_St/x^2$, where D_S is the diffusion coefficient of sulfur at a given temperature, t is time, and x is sample thickness. Scale adhesion in 1100 °C cyclic oxidation tests was mapped as a function of annealing condition, sample thickness and sulfur content. The results indicated that adhesion was maximized when the bulk sulfur content was reduced below that corresponding to an equivalent accumulation of 1 monolayer of segregated sulfur. For 0.5 mm samples, a critical sulfur content of ~0.4 ppmw was calculated.

Above this value, moisture-induced spallation is observed; below, it is insensitive. As an illustration of the sulfur dependence of MIDS, sample weights were recorded before and after exposure to moist breath or water immersion at 40, 200, and 500 cycles, Figure 19. It is seen that greater amounts of MIDS (up to 0.6 mg/cm^2) correlate with higher sulfur contents (5 to 7 ppmw S), and spallation decreases to almost the noise level below about 0.4 ppmw S. This is in accord with the schematic behavior shown in Figure 3, where the MIDS amount (curve *B* minus curve *A*), shrinks at lower sulfur contents. It is also noted that increased scale thickness and scale damage results in a corresponding MIDS increase as oxidation progressed from 40 to 200 hr. This is equivalent to translating the envelope for MIDS, curve *B*, to lower sulfur contents because of higher stain energy and scale damage. However, this trend reverses for the 500 hr data. Here, weight losses of 25 mg/cm^2 have already been achieved for the high sulfur samples.

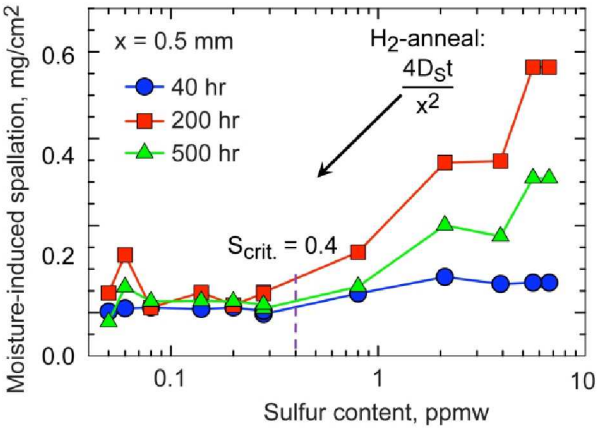

Figure 19.—Effect of sulfur content on the amount of moisture-induced spallation after cyclic oxidation of PWA1480 at 1100 °C, 1-hr cycles (Ref. 45).

Thus they have transitioned to less protective oxides, more spallation upon immediate cool-down, and less residual strain energy. This can be visualized as translating curve *A* to lower sulfur contents and convergence with curve *B*. Nevertheless, the overall trend of Figure 19 follows a similar trend as those shown in Figure 12 for hydrogen-induced, sulfur-contaminated, Ni grain boundary embrittlement. Note also that a lower limit of about 0.04 monolayer of sulfur was necessary for Ni embrittlement, even with substantial H charging. This corresponds in like manner to the lower limit of 0.4 ppmw sulfur in the MIDS curves for PWA 1480, the implication being that lower bulk sulfur contents translate into reduced segregation levels.

Thermal Barrier Coatings

Given the direct effect of alumina scale spallation on TBC life, moisture effects can be expected for TBC's relying on alumina-forming bond coats. Indeed, such a phenomenon was first reported as blistering of a PVD-TBC over a pre-oxidized commercial Ni(Pt)Al bond coat (Ref. 52). Since the delamination was verified to be at the scale-metal interface by photoluminescence piezospectroscopy, it was surmised that moisture-assisted slow crack growth was the operative process, analogous to moisture-assisted slow crack growth in bulk alumina.

Moisture effects were monitored for 250 μm plasma sprayed TBC's tested in conventional cyclic oxidation (Ref. 54). Here PWA 1484 substrates were used without a bond coat to exhibit a more direct effect of substrate sulfur content on scale adhesion and TBC life. Life was found to increase from 200 to 2000 cycles by decreasing the sulfur content from 1.2 to 0.01 ppmw. Furthermore, of the 8 surfaces coated, 6 failed by delayed desk-top spallation (DTS). On the 0.01 ppmw S sample, one failed upon cool down, (marked CD) and one surface did not fail until immersed in water (marked H_2O).

Similar tests were performed for commercially applied PVD YSZ coatings, with a Pt-aluminide bond coat, on René N5 substrates (Ref. 60). Thermal cycling inevitably resulted in DTS for all 6 coatings tested at both 1135 °C with 45 min cycles and at 1150 °C with 60 min cycles. Failure occurred only after removal from the test apparatus and exposure to true ambient conditions, room temperature and relative humidity. In some cases the coatings could be made to fail simply by the application of a water drop. A video recording has been made of another sample that remained intact after cool-down, but then failed completely within 10 sec of applying two water droplets (Ref. 60). The phenomenon has been verified by Rudolphi, Renusch, and Schütze for a low pressure plasma sprayed NiCoCrAlY bond coat followed by an EB-PVD TBC, preoxidized at 1050 °C for 310 hr (Ref. 61). Their results also show acoustic emission triggered by the water drop application and complete failure within 5 sec. This is in contrast with the absence of acoustic emission (AE) or spallation for as-coated samples treated identically.

As a demonstration of this phenomenon, we report on a recent video of a TBC failure for a 1st stage, high pressure turbine blade, pulled from actual engine service. Approximately 1 cm high chord sections were machined from the blade and these were further sectioned into ~1 cm wide samples. The cleaned samples were placed in a alumina boat, oxidized at 1200 °C, and weighed at intervals of 1, 5, 10, 15, and 20 hr. Some sections failed upon cool-down. If a section did remain intact, a water drop was applied by means of a wash bottle. At least one section failed at each examination time after 1 hr. A sequence of still-frames captured from one failure video is shown in Figure 20 for a 15 hr exposure. The first frame shows the application of the water stream, i.e., 0.0 sec. The superimposed time code is in units of [hr:min:sec:1/30 sec]. After 21 sec of moisture exposure, coating delamination initiates at the upper right corner (arrow). A corresponding chip spalled in the next 0.3 sec. In the next 0.2 sec, adjacent sections delaminate explosively and are caught in mid-flight along with some water droplets (arrows). Most of the spallation is complete in another 0.2 sec, with the stable resting appearance obtained in the final 1/2 sec frame. This 1 sec total sequence documents the dramatic nature of moisture-induced TBC failure. It underscores the potential critical nature of moisture effects for coatings and scales reaching high levels of stored strain energy. There is little possibility of true slow crack growth according to classic chemical hydroxylation of alumina. It appears that the interface had been sufficiently weakened during the 21 sec immersion and was ready to fail upon any crack initiation.

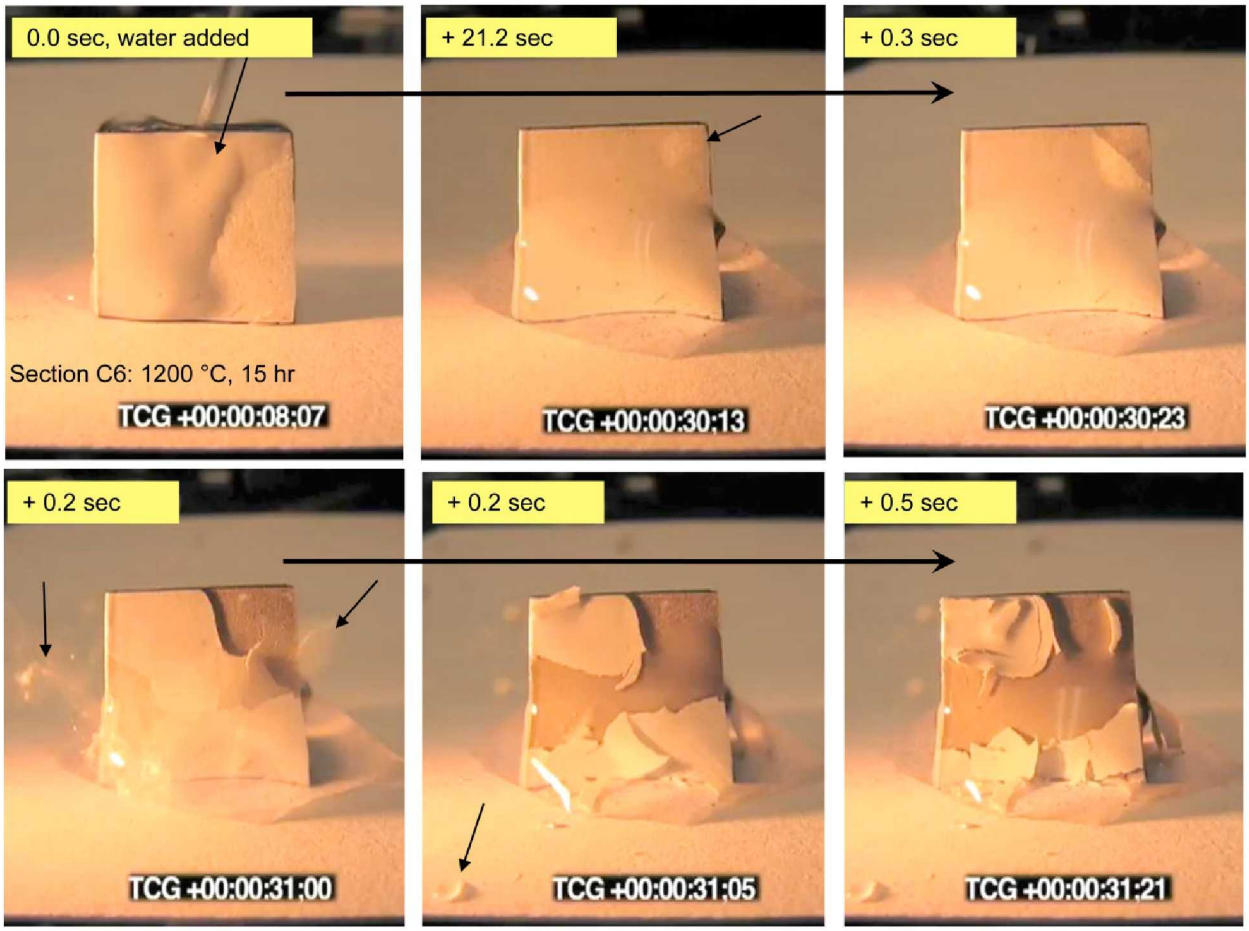

Figure 20.—Water-induced spallation of an EB-PVD TBC on a commercial DS superalloy turbine blade pulled from service and oxidized at 1200 °C for 15 hr. Approximately 1×1 cm trailing edge section; 20 sec incubation, 1 sec spallation times.

Many TBC DTS characteristics are unambiguously elucidated and confirmed in the recent thorough study of Deneux et al. (Ref. 64). Here duplicate samples of conventional EB-PVD TBC samples, using a Ni(Pt)Al bond coat on 0.5 ppmw sulfur AM1 superalloy, were exposed in cyclic furnace tests at 1150 °C. The thermal cycle was 45 min. hot duration, 15 min. forced air cooling to 80 °C. Successive exposures, ranging from 75 to 360 cycles, established a threshold water drop delamination life of ~170 cycles, considered as the most dependable or "real" lifetime. However, coatings survived 200 cycles of normal cycling when maintained in the furnace environment. When the latter samples were exposed to ambient humidity at room temperature, the coatings failed by DTS in a few minutes (or within 38 sec after applying a water drop). Furthermore, coatings stored in dry air at room temperature survived, metastably, for 48 hr., as they too failed within a few minutes after subsequent exposure to ambient humidity. Microstructural examination also revealed cracks in the γ'-$(Ni,Pt)_3Al$ coating surface, which can be considered as further evidence in support of the proposed hydrogen embrittlement mechanism.

Their study underscores a potential uncertainty or drawback to current TBC furnace cycle test protocol. If the samples are allowed to remain at furnace test conditions, they may give misleading spallation lives. Alternatively, intrinsic scatter will be built into this life test depending on any variance of exposures to ambient conditions (such as remote inspection or sample weighing) and the relative humidity of the locality or laboratory environment. It has been argued that relative humidity can be increased by about a factor of 40x in removing a sample from a 100 °C environment and cooling to ambient conditions, because of the high saturation moisture level at 100 °C compared to that at 21 °C (Ref. 3).

H Detection Under Alumina Scales

Support for MIDS by hydrogen detection under a mature alumina scale due to moisture exposure is a difficult task. First, detection through a thick scale is problematic, especially considering interface roughening due to sputter profiling for spectroscopy. Secondly, detection directly after exposure of an interface to moisture is a problem for high vacuum systems. Given these issues, alternative or modified techniques may be required. In that regard, an effort was undertaken to detect hydrogen under an alumina scale formed on a vacuum plasma sprayed NiCoCrAlY bond coat, with an air plasma spray TBC. Oxidation was performed at 1100 °C for 75 to 1200 hr. (Refs. 59 and 63). Hydrogen was analyzed by a specialized proton- induced gamma emission (P.I.G.E.) technique. Basically, ^{15}N ions are used to bombard the sample and identify H by the emission of gamma rays according to the nuclear reaction $^{1}H(^{15}N, \alpha\gamma)^{12}C$ with a sharp resonance et a 15N-energy of 6.385 MeV. Samples were exposed in dry or 2.5, 10 and 50v/o H_2O moist air. The interface was exposed by a 4-pt. bend fracture inside a specially built vacuum chamber to avoid contamination with water vapor from the laboratory environment. Generally a hydrogen signal corresponding to 0.1 to 2 at.% was detected a few hundred nm into the metal, but with no distinguishable interfacial concentrations, other than a system-generated peak. Furthermore, at this time, no large differences between the dry and wet oxidation samples was obtained, Figure 21. There may be a basic difference in hydrogenation behavior between the isothermal oxidation in moist air (studied here) and cyclic oxidation followed by exposure to ambient humidity (generally required to give rise to MIDS and DTS phenomena). These techniques are valuable for detecting how and when hydrogen may segregate at the scale metal interface.

Glow Discharge Optical Emission Spectroscopy (GD-OES)

Following the results discussed for anodic films, GDOES has recently been attempted to characterize H-profiles for pre-formed thermal scales that had been exposed to hot water (Ref. 68). In this preliminary attempt, samples of René N5 were oxidized at 1150 °C for 5 hr in flowing argon ($pO_2 \approx 2\times10^{-4}$ atm.) to minimize transient Ni-scales). The oxidation mass gain was approximately 0.2 mg/cm^2, which is equivalent to ~1.1 μm of Al_2O_3. At this thickness the scale is translucent and not especially vulnerable to high strain energy or spallation. The sample was exposed to water heated at 90 to 100 °C for 100 hr. in an effort to charge the material with hydrogen according to the proposed mechanism. No mass change occurred from the water treatment. It was then stored in room temperature water for about 2 weeks, until

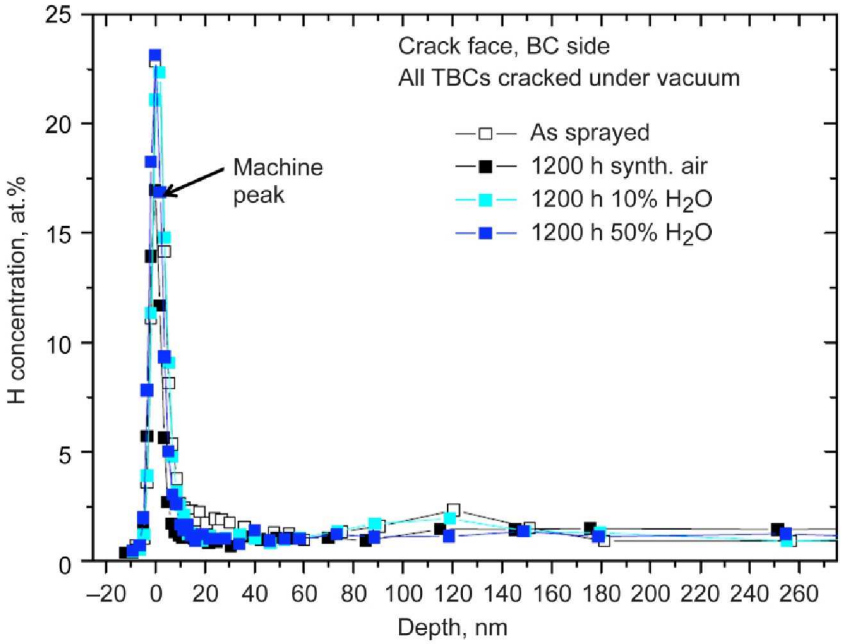

Figure 21.—P.I.G.E. hydrogen concentration profiles in a NiCoCrAlY bond coat before and after oxidation in 1100 °C air at various moisture contents. TBC removed by in situ 4-pt. bend. Initial peak is interpreted as a chamber artifact (used with permission from Ref. 63).

the GDOES analysis was performed. The analysis technique had been proven to characterize 30 to 300 nm alumina scales formed on γ′-Ni_3Al (Pt, Hf) alloys with excellent resolution (Ref. 69). The present results are shown in Figure 22. The H profile exhibits a large drop from adsorbed surface moisture, then a small peak at the scale-metal interface. Another sample, pre-oxidized for only 2 hr in 5%H_2/Ar ($pO_2 \approx 10^{-16}$ atm), gained 0.06 mg/cm^2 (~0.3 μm of Al_2O_3), and exhibited no internal peak. It remains to be seen whether samples with no moisture exposure can still exhibit an interfacial H-peak or whether the moisture treatment is necessary to produce interfacial H. In any event, this preliminary evidence suggests moisture-induced interfacial H segregation may exist for alumina scales.

Pd-Al_2O_3 Interface Trapping of Hydrogen

Electrochemical polarization studies of internally oxidized Pd-3 at.% Al alloys were used to study the energetics of hydrogen trapping at the aluminum oxide-metal interface (Ref. 70). Since Pd and Ni are completely soluble and have identical crystal structures, these findings would be expected to be insightful to the Ni-Al_2O_3 metal-scale interface as well. Using cathodic charging (coulometric titration) and reverse anodic polarization, irreversible (stable) trap saturation values of 700 ppma were established. Given the distribution and geometry of the internal precipitates, this approximated one hydrogen atom for every oxygen atom on the (0001) close-packed basal habit plane (i.e., one monolayer). Accordingly, H diffusivity was measured to drop significantly when the hydrogen concentration was below saturation values for trapping. A binding energy of ~ –200 kJ/mole of H was estimated for these traps.

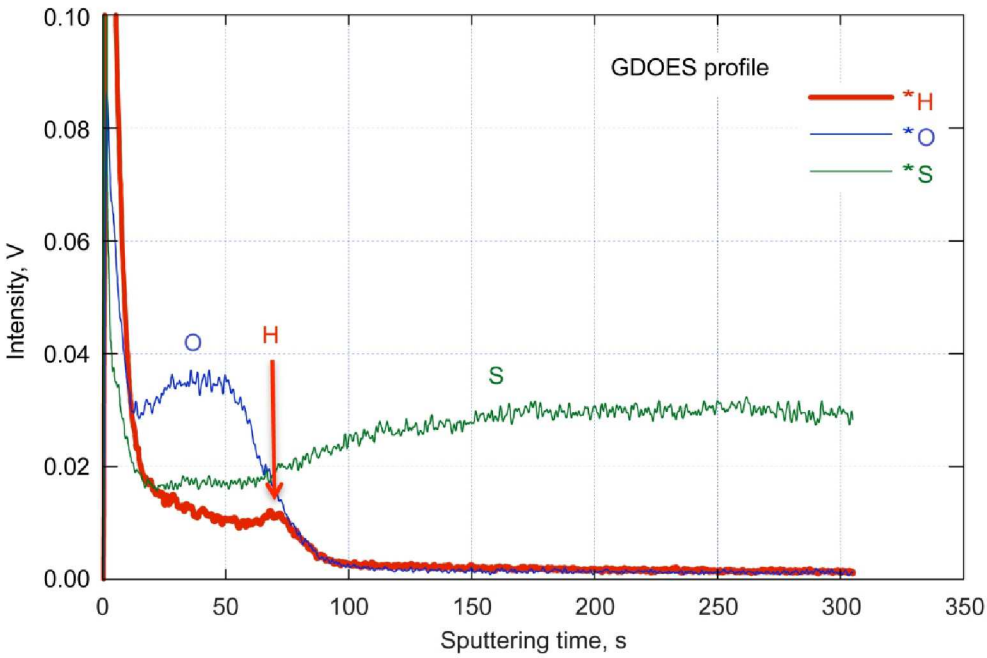

Figure 22.—GD-OES hydrogen profile for a scale produced on René N5+Y, then submerged in 90 to 100 °C water for 100 hr (Ref. 68).

Supporting Critical Experiments

Electrolytic Cathodic Charging

Electrochemical hydrogen injection techniques are often used to demonstrate hydrogen embrittlement. Since hydrogen had been proposed as the key factor responsible for MIDS and DTS according to the reaction shown in Equation (2) above (Ref. 2), cathodic charging was then attempted to support the hypothesis. Thus, well characterized samples of René N5+Y, pre-oxidized at 1150 °C for 1000 1-hr cycles, immersed in water to leave only highly adherent scales (Refs. 53 and 55), were later subjected to hydrogen charging in 1N H_2SO_4, a commonly employed electrolyte. In order to minimize gaseous H_2 evolution, the current versus voltage response was carefully mapped in 0.1 V increments. It was found that at ~ –2.0 V, a measurable current was first observed, amounting to ~0.5 mA. This is a relatively benign condition compared to the typical 50 to 100 mA currents employed for cathodic charging of bulk material. Samples charged at –2.0 V were examined intermittently and weighed for hold-times of ~10 min. up to 1 hr., both before and after applying the voltage.

Simple immersion in the electrolyte, without any applied potential, produced no additional spallation, as shown in Figure 23. However, measurable weight loss resulted from cathodic charging. This decayed with time, as all the scale was removed, with no particular correlation of loss rate with current. Optical macrographs revealed successive areas of spallation with time, the limits shown by the start/finish insets, confirming that the weight loss was due to scale removal. Subsequent SEM studies identified the characteristic alumina grain imprints in the exposed metal interface (Ref. 2).

Further supporting evidence is provided by the catastrophic swelling and cracking for a bare René N5+Y sample subjected to overcharging at –3.0 V and ~100 mA, Figure 24. Here it can be seen that the alloy was severely blistered and cracked at many levels, even etched down to the scale of individual γ′particles. Indeed, some degree of hydrogen embrittlement has been reported for fatigue tests of the superalloy PWA1480 resulting from high pressure hydrogen charging (Refs. 71 and 72). As a further note added in proof, reverse (anodic) polarization, at the respective +1.3 V knee, resulted in slow, but continuous weight loss primarily due to alloy dissolution, producing a closely correlated weight loss

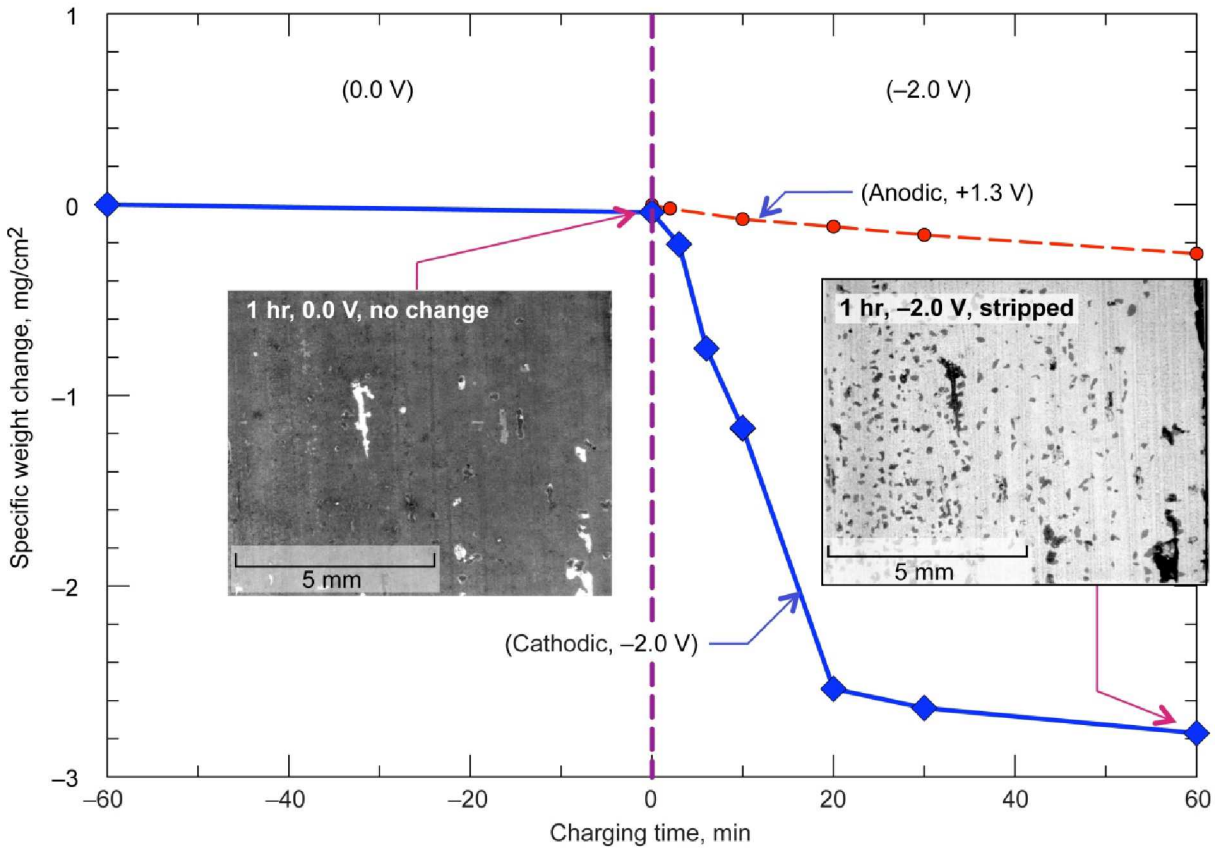

Figure 23.—Cathodic hydrogen charging and descaling of René N5+Y. Hydrogen annealed at 1250 °C for 100 hr prior to oxidation at 1150 °C for 1000 1-hr cycles. No spallation after 1 hr immersion in 1N H_2SO_4 with no applied voltage. Complete stripping in 20 min at –2.0 V, 0.5 to 1.0 mA charging (Ref. 2).

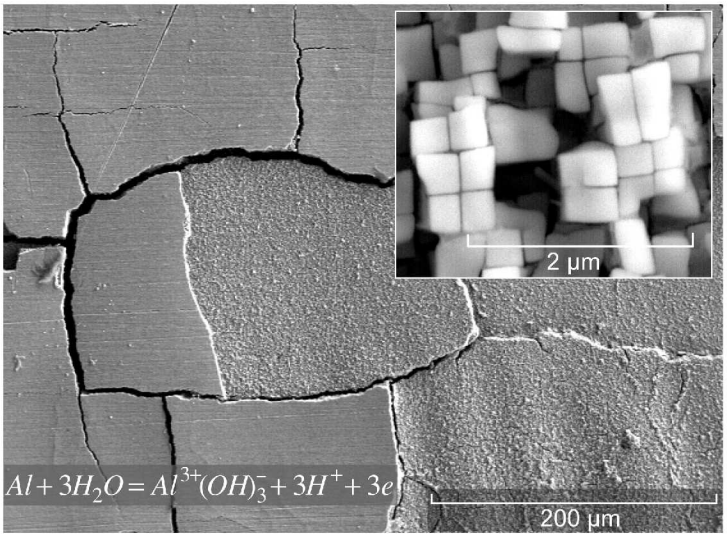

Figure 24.—Massive blistering, cracking, and etching of unoxidized René N5+Y subjected to cathodic hydrogen overcharging at –3.0 V, ~100 mA (Ref. 2).

rate–current dependence (Ref. 2). All in all, this set of experiments was consistent with interfacial scale delamination due to hydrogen charging. Accordingly they support the aspect of MIDS and DTS that presumes hydrogen as the key factor in moisture effects.

These experiments are thus related to the cathodic hydrogen charging effects on metals. As mentioned in Section I above, cathodic charging produced brittle behavior in the intermetallic, Ni_3Al, even though it was ductilized by doping with B and Zr (Refs. 29 and 30). It is also recalled that Jones used cathodic charging to establish a clear additive effect of H+S grain boundary embrittlement of Ni (Ref. 36), as shown on a plot of grain boundary embrittlement plot as a function of hydrogen charging potential and sulfur grain boundary segregation, Figure 12. Now we compare those potentials and embrittlement response with that used for descaling. Such potentials give a measure of the hydrogen levels injected into the materials. The range employed by Jones for Ni grain boundary embrittlement was –0.30 to –0.72 V, measured against a saturated calomel Hg/Hg/Cl electrode (SCE) (Ref. 36). For the descaling experiments, it was determined that the critical voltage of –2.0 V, used for the René N5+Y samples polarized against a Pt electrode, corresponded to –0.40 V measured against a saturated Ag/AgCl reference electrode (Ref. 73). From tables of standard reference electrodes potentials, it is seen that the SCE is 0.045 V more positive than Ag/AgCl. This translates to a corresponding differential of –0.445 V SCE for the descaling experiment. This potential can be used to interpolate the sigmoidal curve fit parameters from the three fitted curves (solid blue, fuschia, and green) of Figure 12, giving the result shown as the dashed red curve. The sigmoidal curve fits for the experimental and interpolated curves for equation (5) are given in Table 2, where

$$\mathrm{GBF} = \frac{a}{1 + \exp\dfrac{\left(-\left(S - S_0\right)\right)}{b}} \tag{5}$$

a and *b* are function parameters and S is the sulfur coverage, in monolayers.

TABLE 2.—SIGMOIDAL CURVE PARAMETERS FOR EQUATION (5) USED TO DESCRIBE CATHODIC CHARGING EMBRITTLEMENT OF NI (REF. 36) AND INTERPOLATED VALUES FOR CATHODIC DESCALING OF RENÉ N5 (REFS. 2 AND 73)

	–0.30 V	–0.445 V	–0.56 V	–0.72 V
a	96.857	95.600	95.296	95.290
b	0.0406	0.0290	0.0250	0.0181
S_o	0.195	0.127	0.081	0.041
R^2	0.999	-------	0.999	0.997

While specific interfacial sulfur had not been measured for the René N5+Y alloys, it had been estimated to produce a maximum of 0.15 monolayers of sulfur by simple oxidative recession, assuming rejection of sulfur from the growing scale (1000 hr at 1150 °C) (Ref. 74). This is presented as the diamond symbol on the estimated curve. It is seen to fall well within the E-S range shown by Jones to embrittle Ni grain boundaries, corresponding to ~65 percent GBF. This supports the parallelism between Ni grain boundary embrittlement and Ni-alumina scale interfacial spallation. It further reinforces the combined detrimental effect of sulfur and hydrogen segregation on scale adhesion.

A further comparison of the Jones E-S embrittlement plot can be made against the moisture -induced scale spallation discussed for PWA 1480 in Figure 19. Here additional moisture -induced spallation at 40, 200, and 500 hr was shown to increase with the bulk sulfur content. Some convergence with the Ni embrittlement data is addressed in Figure 25 by estimating a corresponding segregation level, θ_S, for samples with various bulk sulfur contents, C_S. These were approximated from the Langmuir-McLean

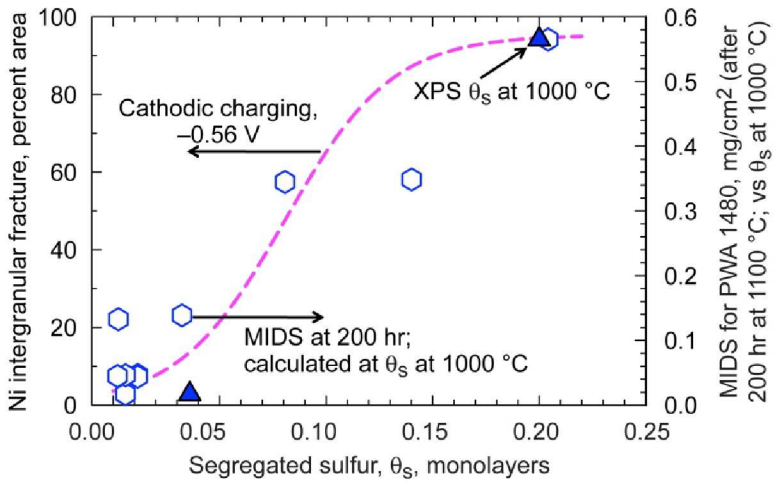

Figure 25.—Comparison of sulfur effects on moisture induced spallation (PWA1480, from Fig. 19) and hydrogen induced GBF (Ni, from Fig. 12). PWA 1480 segregated sulfur estimated from 1000 °C data (Refs. 76 and 77). GBF data for cathodic potential of –0.56 V (from Fig. 12 (Ref. 36)).

isotherm from Auger measurements of Miyahara et al. (Ref. 75), and XPS (x-ray photoelectron spectroscopy) surface segregation levels measured by Jayne and Smialek (Ref. 76), and reconstructed in (Ref. 77):

$$\frac{\theta}{1-\theta} = 0.19\, C_S \exp\{137 kJ / RT\}$$

Since the segregation level is temperature dependent, a single temperature producing closest agreement with that measured by angle-resolved XPS (i.e., 1000 °C), and likely to be quenched in upon cool-down, was chosen for this exercise. Also, the maximum MIDS data, corresponding to that measured after 200 hr of oxidation was plotted (right axis). In juxtaposition, the well developed sigmoidal GBF curve from Jones (Ref. 36), corresponding to –0.56 V cathodic charging, was selected (left axis). It is acknowledged that these two families of data represent, to some extent, arbitrarily chosen cathodic charging potentials (for Ni) and oxidation time and segregation temperature (for PWA1480). Other charging conditions may result in truncated sigmoidal curves, skewing them to one extreme of the sulfur range. Other segregation temperatures may result in more divergence at a given bulk sulfur level. Nevertheless, the parallelism of these specific GBF and MIDS behaviors are apparent, both indicating a synergism between hydrogen and sulfur. This again suggests the phenomenological similarity between grain boundary embrittlement of Ni and moisture-induced interfacial alumina scale spallation.

High Temperature H_2O Causes H to be Incorporated Into Scales and Alloys

As evidence that hydrogen can enter alloys and reach critical levels, we cite the work of Subanovic et al., in which a plasma sprayed sample of NiCoCrAlY was oxidized in an Ar–4%H_2–2%H_2O gas (Ref. 78). Here oxidation at 1100 °C for 72 hr allowed H to penetrate the scale along Y-rich yttrium aluminum perovskite (YAP) $YAlO_3$ oxide stringers and reach the metal. This continuous process eventually resulted in swelling and blistering of the sample from H_2 gas pressure, Figure 26. It was found that both H_2 and H_2O components were required to produce swelling, indicating that the moisture reaction with Al (Eq. (1)) was again involved. In this case, the reaction was at high temperature where hydrogen solubilities and diffusion are substantially increased. So instead of just local damage at the scale-metal interface, hydrogen was able to reach much higher levels in the bulk volume of the metal.

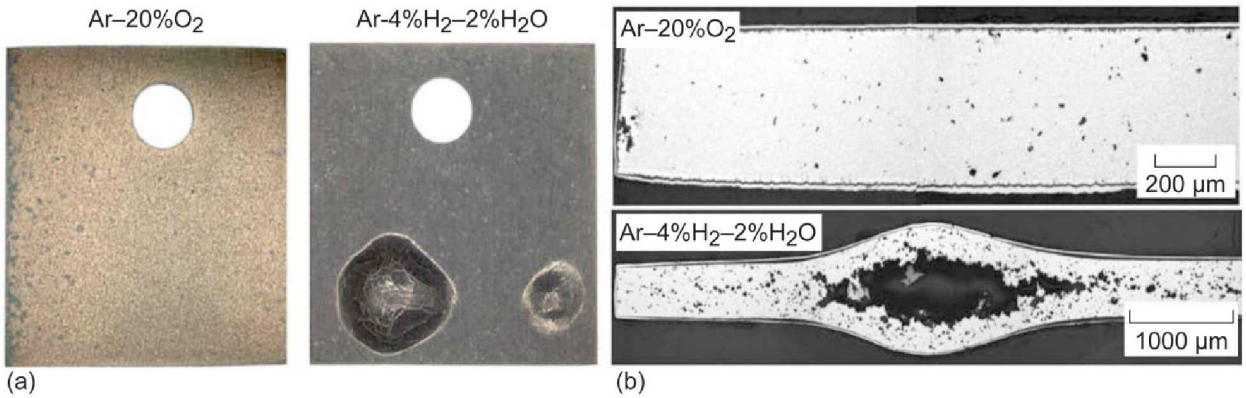

Figure 26.—Catastrophic internal voidage and swelling for free-standing plasma sprayed sample of NiCoCrAlY oxidized in an Ar–4%H_2–2%H_2O gas at 1100 °C for 72 hr (used with permission from Ref. 78). Oxidation in Ar–20%O_2 produced no such unusual effect. (a) Optical macrophotos of exposed surfaces. (b) SEM micrographs of cross sections.

It is recalled that a SUS 430L stainless steel, oxidized at 900 °C for 6 hr in N_2–2.4%O_2–19.7%H_2O, incorporated hydrogen in both the scale and alloy (Ref. 42). It was detected by thermal desorption mass spectroscopy by reheating samples up to 750 °C in vacuum. The maximum amount of dissolved hydrogen in the scale was estimated to be ~0.3 mole%. In addition, the use of glow-discharge optical emission spectroscopy revealed a small, but measurable, hydrogen enrichment in the vicinity of the oxide scale-metal interface.

The embrittlement response of 718PLUS (Ref. 34), described in Section IIIA, also implicates the incorporation of hydrogen during high temperature (704 to 817 °C) exposure to moist environments.

Discussion

It has been shown in Section I that activated aluminum powder reacts with liquid water, generating H_2 gas. We can therefore expect some measure of reaction between adsorbed moisture and Ni-Al alloys, with the potential of a hydrogen by-product. The degree of reaction would likely be much reduced from that of pure aluminum, simply because aluminum activities in these alloys can be orders-of-magnitude lower than the pure element. The reaction can only take place for oxidized samples if the scale-metal interface is exposed by partial spalling or thru-cracks in the scale. Thus, more intact scales are less prone to the moisture effect, with full immunity observed for the most protective.

The ab initio studies discussed in Section II indicate Co-Al_2O_3 interfacial weakening trends by adding H interstitials. Further reductions in the work of adhesion appear possible with interfacial carbon. This is consistent with MIDS on René N5+Y, where moisture effects were more pronounced for as-received material with a higher carbon content. By comparison, hydrogen-annealed samples, which reduced the carbon content, exhibited remarkable MIDS resistance. Also, interfacial toughness measurements of bulk Al_2O_3-Ni samples indicate weakening due to both moisture (in ambient air) and sulfur segregation. Given that Pd-Al_2O_3 internal interfaces act as stable traps for hydrogen atoms, it is reasonable to expect that the alumina scale-metal interface behaves similarly, with the caveat that bulk Pd may serve as a substrate matrix for mobile H diffusion compared to Ni.

The embrittlement of aluminides in ambient (humid) atmospheres provided the original impetus for the present line of thinking (Refs. 1 and 2). The chemical reactivities of bulk intermetallic alloys and that of Ni_3Al phases in bond coats and superalloys are likely to be similar enough to result in the same type of hydrogen formation and adsorption. The embrittlement of Ni_3Al compounds or PWA 1480 and René N5+Y γ/γ' alloys in hydrogen-containing gas or by cathodic hydrogen charging, respectively, suggests that scale interfaces may be sensitive to other sources of hydrogen besides moisture. Indeed, cathodic charging has caused massive interfacial de-scaling of otherwise perfectly adherent scales formed on

hydrogen annealed René N5+Y. It may also be surmised that MIDS and DTS may be avoided in vacuum or dry O_2, as was indeed shown for TBC's (Ref. 64). It has yet to be demonstrated whether and to what degree H_2-containing gases will lead to delayed spallation. They have already produced H_2-induced gas bloating of a conditioned NiCoCrAlY alloy (Ref. 78). Finally, since B and other dopants mitigated the environmental embrittlement of Ni and Fe aluminides, it might be also expected to have beneficial effects regarding MIDS and DTS for thermally-grown alumina scales. Boron is indeed present as a low level dopant in many commercial alloys and coatings.

Thin amorphous alumina films on aluminum are very sensitive to moisture. This provides an extremely close analogy to the case of thermally grown alumina scales on Ni-Al high temperature alloys and coatings. The observation of moisture-induced blisters, de-scaling by H-implantation (not He), and detection of interfacial H under the amorphous films strongly implicate hydrogen as the key to the weakened alumina-aluminum interface. In so far as these observations might apply to MIDS for thermally grown scales, one might expect hydrogen injection by suitably conditioning pre-oxidized samples in hot water and detection by GDOES as shown in a preliminary study, Figure 21 (Ref. 68). Further substantiation by this technique would be warranted and may prove to be decisive. Thus, many of the conditions necessary for MIDS and DTS have been addressed and cross- referenced to other related hydrogen-based phenomena. A source of hydrogen is a pre-condition, as ambient moisture, water immersion, hydrogen gas, or cathodic hydrogen charging. The scale must have some damage, as from extensive thermal cycling, to allow access to an exposed metal interface. The interface should possess a high residual (biaxial tension) stress level, such as would result from a thick scale with high strain energy in cooling from high temperature. Progressive spallation would be time-dependent, allowing for some element of hydrogen diffusion ahead of the damaged area. These effects are most evident in a hypothetical "sensitive zone," where the sulfur content is low enough (or reactive elements high enough) to maintain the scale upon initial cooling, but not so low as to preclude spallation altogether. In that regard, cathodic hydrogen charging was still found to detach the most adherent of scales on hydrogen-annealed René N5+Y, even after it had been immersed in water.

Catalytic effects of S, Pt, Ti, and Y have been briefly discussed with an eye toward H absorption and embrittlement. At first glance, these effects appear in concert with known impurity/doping trends in scale adhesion. However, at this early stage it is difficult to accurately assess these potential composition effects on moisture-induced spallation, independent of purely sulfur effects. In fact, this brings up a basic dilemma to the backdrop of established adhesion phenomena: given that spallation is conventionally observed under ubiquitous ambient conditions, there is no projection for how good adhesion might be *without* moisture. Stated another way, the indigenous significance of moisture to any form of interfacial weakening and alumina scale spallation may be greater than previously recognized. This points to a potential H-S synergy for interfacial weakening. At a minimum, previous studies of hydrogen embrittlement of sulfur contaminated grain boundaries in metals found these impurity effects to be additive (Refs. 34 to 36).

Conclusions

This monograph has attempted to highlight relevant hydrogen-induced weakening phenomena, often derived from moisture, from a number of related fields and apply them to the scale spallation issue. Following the logic tree presented in Figure 1, we have started with the basic reactivity of liquid water with activated aluminum metal, showing that hydrogen gas is yielded as a by-product. Detrimental hydrogen effects were predicted by ab initio oxide-metal interface calculations and born out experimentally in fracture mechanics studies of alumina-Ni bonded samples under moist conditions. Ambient humidity has also embrittled aluminides and other intermetallics, again producing H as a by-product of reactive aluminum and water. Time-sensitive (strain rate) properties were consistent with hydrogen diffusion as a pre-requisite for embrittlement. Grain boundary interfacial failure was a common attribute, and hydrogen was detected in the bulk alloy. Thin native, electropolished, or anodic aluminum oxide films on aluminum alloys were sensitive to scale-metal blistering simply by exposure to room

temperature moisture. Again, hydrogen was implicated because the moisture-treated films revealed a hydrogen concentration at the film-metal interface by various techniques. Finally hydrogen, but not He, implantation was also capable of delaminating these films, independently of moisture.

Many studies of moisture-induced scale spallation and desk-top spallation of TBC's now exist. Various researchers have investigated systems exhibiting the "sensitive zone" of a scale or TBC system with relatively good adhesion, but compromised by having some cyclic damage and the high strain energy of a mature scale. The key condition is to retain the scale upon normal cool-down or in the low humidity of the furnace environment, then produce a time-delayed failure by unintentional or deliberate exposure to higher relative humidity. Dedicated, sophisticated efforts are underway to identify hydrogen under the scale as a result of these moisture reactions. In any event, auxiliary exposures, by cathodic hydrogen charging or exposure of a special microstructure to an $Ar\text{-}H_2\text{-}H_2O$ mixed gas, have produced remarkable results, e.g., complete de-scaling or catastrophic blistering of the alloy, respectively. Both results have been attributed to hydrogen-driven phenomena. In all, the 'logic tree' structural approach has arranged many findings that, at present, appear in concert with the proposed mechanism that hydrogen embrittlement is the root cause of moisture-induced spallation of protective alumina scales.

Thus, the primary point of this paper was to structure the circumstantial evidence to first identify and isolate hydrogen as the most probable cause. A more detailed model cannot be presented until the critical factors are fully identified and studied. The situation is analogous to the direct sulfur effect as opposed to the indirect reactive element effect on scale adhesion. The latter entailed many proposed mechanisms, among which sulfur-gettering arose as the most critical. It is recognized that the proposed model is far from complete as a logical description of what the atomistic details of the hydrogen mechanism might be. These may hopefully be revealed in further dedicated studies directed toward hydrogen-driven phenomema, e.g., measuring properties as a function of the hydrogen reactivity, fugacity, and diffusion. In that regard, it is recalled that hydrogen embrittlement of metals has been discussed in terms of weakened metal bonds and interfaces, enhanced local plasticity or decreased dislocation mobility, internal pressure and swelling, and hydrogen bubbles or brittle hydrides. It is worth acknowledging that after 70 years of recognizing and studying the problem, with strong evidence for each, there is still no single hydrogen embrittlement mechanism that is universally accepted as dominant in all cases.

References

1. J.L. Smialek, "Moisture Induced Spallation and Interfacial Hydrogen Embrittlement of Al_2O_3 Scales," NASA/Technical Memorandum, 2005-214030, December, 2005.
2. J.L. Smialek, *JOM*, 1, 29-36 (Jan., 2006).
3. J.L. Smialek, Moisture Induced Delayed Spallation of Alumina Scales on a Ni(Pt)Al Coating, Oxid. Met., 72 (2009) 259–278.
4. J.L. Smialek: "Maintaining Adhesion of Protective Al_2O_3 Scales," *JOM*, Jan. 2000, 22–26.
5. Z.Y. Deng, Y.F. Liu, Y. Tanaka, J. Ye, and Y. Sakka, J. Amer. Ceram. Soc., 88 (2005) 977–979.
6. Z.Y. Deng, Y.F. Liu, Y. Tanaka, H.W. Zhang, J. Ye, and Y. Kagawa, J. Amer. Ceram. Soc., 88 (2005) 2975–29779.
7. Z.Y. Deng, J. Ferreira, Y. Tanaka, and J. Ye, J. Amer. Ceram. Soc., 90 (2007) 1521–1526.
8. H.A. Al-Abadleh and V.H. Grassain, Langmuir, 19 (2003) 341–347.
9. G. Hultquist, et al., Catal. Lett., Volume 132, Issue 3 (2009), Page 311.
10. S.Y. Hong, A.B. Anderson, J.L. Smialek, Surface Science, 230 (1990), 174–183.
11. W. Zhang, J.R. Smith, X-G. Wang, and A.G. Evans, Phys. Rev. B 67 (2003) 245414.
12. I.J. Bennett, J.M. Kranenburg, and W.J. Sloof, J. Am. Ceram. Soc. 88 (2005) 2209–2216.
13. J.R. Smith, Y. Jiang, and A.G. Evans, Int. J. Mat. Res. 98 (2007), 1214–1221.
14. W. Zhang, J.R. Smith, and A.G. Evans, Acta Mat., 50, (2002), 3803–3816.
15. X.G. Wang, J.R. Smith, and M. Scheffler, J. Am. Cerm. Soc., (2003) 696–700.
16. X.G. Wang and J.R. Smith, Physical Review B, 70 (2004) 081401.
17. Y. Jiang, J.R. Smith, and A.G. Evans, Applied Physics Letters, 92 (2008) 141918.

18. A.G. Evans, J.W. Hutchinson, and Y. Wei, Acta mater., 47 (1999) 4093–4113.
19. F. Gaudette, S. Suresh, A.G. Evans, G. Dehm, and M. Ruhle, Acta mater. 45 (1997) 3503–3513.
20. F.G. Gaudette, S. Suresh, and A.G. Evans, Metall. Mat. Trans., 31A (1999), 1977–1983.
21. J.S. Wang and A.G. Evans, Acta mater. 46 (1998) 4993–5005.
22. D.A. Bonnell and J. Kiely, phys. stat. sol., 166 (1998) 7–17.
23. N.S. Stoloff and D.J. Duquette, *JOM*, 45, (1993) 30–35.
24. C.T. Liu, "Ni_3Al Aluminide Alloys," in *Structural Intermetallics*, R. Darolia, et al., eds., TMS, Warrendale, PA, 365–377, (1993).
25. N.S. Stoloff, "Hydrogen and Moisture-Induced Embrittlement of Nickel and Iron Aluminides, in *Hydrogen Effects in Materials*, A.W. Thompson, N.R. Moody, eds., TMS, Warrendale, PA, 523–537 (1996).
26. G.L. Chen and C.T. Liu, International Materials Reviews, 46 (2001) 253–270.
27. C.T. Liu, E.H. Lee, and C.G. McKamey, *Scripta Metall.*, 23, (1989) 875–880.
28. C.T. Liu, C.G. McKamey, and E.H. Lee, Scripta met., 24 (1990) 385–390.
29. A.K. Kuruvilla and N.S. Stoloff, Scripta met. (1985) 83–88.
30. A.K. Kuruvilla and N.S. Stoloff, "Hydrogen Embrittlement of Ordered Alloys," in Mat. Res. Soc. Symp. Proc. 39 (1985) 229–238.
31. E.P. George, C.T. Liu, D. Pope, Scripta metall. mat., 30 (1994) 37.
32. E.P. George, C.T. Liu, and D.P. Pope, Scripta metall. mat., 44 (1996) 1757.
33. K.H. Lee and C.L. White, Scripta metall. mat., 33 (1995) 129.
34. R.W. Hayes, Met. Mat, Trans., 39A (2008) 2596–2606.
35. A. Kimura and H.K. Birnbaum, Acta Metall., 36 (1988) 757–766.
36. R.H. Jones, in Hydrogen Effects on Material Behavior," N.R. Moody, W. Thompson, eds., TMS, Warrendale, PA., (1990) 817–843.
37. G.M. Scamans, J. Mat. Sci., 13 (1978) 27–36.
38. G.M. Scamans and A.S. Rehal, J. Mat. Sci., 14 (1979) 2459–2470.
39. K. Shimizu, H. Habazaki, P. Skeldon, G.E. Thompson, and G.C. Wood, Surf. Interface Anal. 27 (1999) 998–2002.
40. K. Shimizu, G.M. Brown, H. Habazaki, K. Kobayashi, P. Skeldon, G.E. Thompson, and G.C. Wood, Electrochemica. Acta. 44 (1999) 2297–2306.
41. L. Iglesias-Rubianes, P. Skeldon, G.E. Thompson, U. Kressig, D. Grambole, H. Habazaki and K. Shimizu, Thin Solid Films. 424 (2003) 201–207.
42. A. Yamauchi, Y. Yamauti, Y. Hirohata, T. Hino, and K. Kurokawa, "TDS Measurement of Hydrogen Released from Cr_2O_3 Scale Formed in N_2-O_2-H_2O Atmospheres," High Temperature Corrosion and Materials Chemistry, Proc. Electrochem. Soc., E. Opila, T. Maruyama, T. Narita, E. Wuchina, J. Fergus, J. Mizusaki, and D. Schifler, eds., The Electrochemical Society, Pennington, NJ, (2004) 93–100.
43. Y. Liu, M. Alexander, E. Koroleva, P. Skeldon, G.E. Thompson, P. Bailey, T.C.Q. Noakes, K. Shimizu, and H. Habazaki, Surf. Interface Anal. 33 (2002) 318–321.
44. P. Bailey, T.C.Q. Noakes, Y. Liu, M.R. Alexander, E.V. Koroleva, P. Skeldon, G.E. Thompson, H. Habazaki, K. Shimizu, Nuclear Instr. Meth. in Phys. Res. B. 197 (2002) 265–270.
45. J.L. Smialek, Materials Science Forum, Vols. 595–598 (2008) pp. 191–198. (Also NASA/TM—2008-215206. June 2008, 9 pages).
46. J.L. Smialek: "Adherent Al_2O_3 Scales Formed on Undoped NiCrAl Alloys," N.L. Peterson Mem. Symp. Proc. on Oxidation and Associated Mass Transport, TMS-AIME Oct. 6–9, 1986, pp. 297–313.
47. D.R. Sigler, *Oxidation of Metals*, 40, 555–583 (1993).
48. M.A. Smith, W.E. Frazier, and B.A. Pregger, *Mat. Sci. Engineer.*, A203, 388–398 (1995).
49. V. Sergo and D.R. Clarke, *J. Amer. Ceram. Soc.*, 81 [12] (1998) 142–161.
50. J.L. Smialek: "Toward Optimum Scale and TBC Adhesion on Single Crystal Superalloys," High Temperature Corrosion and Materials Chemistry, E.J. Opila, P.Y. Hou, D. Shores, M. McNallan, and R. Oltra, eds., Proc. Electrochem. Soc., Pennington, NJ, 98–9, (1998) 211–220.

51. R. Janakiraman, G.H. Meier, and F.S. Pettit, *Metall. Mat. Trans.*, 30A, (1999) 2905–2913.
52. V. Tolpygo, D.R. Clarke, *Mater. Sci. Eng.*, A278, (2000) 142–161.
53. J.L. Smialek and B.A. Pint, *Mater. Sci. Forum*, 369–372, (2001) 459–66. (also NASA/TM—2000-210362).
54. J.L. Smialek, *Ceramic Engineering and Science Proceedings*, 23, 4, (2002) 485–495.
55. J.L. Smialek and G.N. Morscher, *Mater. Sci. Engineer. A*, 332 (1–2), (2002)11–24.
56. M.C. Maris-Sida, G.H. Meier, and F.S. Pettit," *Metall. Trans.*, 34**A**, (2003) 2609–2619.
57. D. Renusch, H. Echsler, M. Schütze: Mat. High Temp., 21 (2004), 65–76.
58. K. Onal Hance, "Effects of Water Vapor on the Oxidation Behavior of Alumina and Chromia Superalloys between 700 °C and 1000 °C," Ph.D. Thesis, U. Pittsburgh (2005).
59. H. Zschau, M. Dietrich, D. Renusch, M. Schütze, J. Meijer, H. Becker, *Nucl. Instr. Met.B*, 249, (2005) 381–383.
60. J.L. Smialek, Dongming Zhu, and Michael D. Cuy, Scripta mat., 59 (2008) 67–70; also NASA/TM—2008-215210, (April, 2008).
61. M. Rudolphi, D. Renusch, M. Schütze, *Scripta mat.*, 59 (2008) 255–257.
62. M. Rudolphi, D. Renusch, H.-E. Zschau, and M. Schütze, Materials Science Forum, Vols. 595–598 (2008) 177–184.
63. M. Rudolphi, D. Renusch, M. Schutze, and J. Meijer, DECHMA Final Report Abschlussbericht DFG-Re 2653/1–2, "The Role that Hydrogen and Sulfur Play in Desktop Failure of Thermal Barrier Coatings," Jan. 2010, also paper 2009-D-09-00171presented at ICMC-TF.
64. V. Deneux, Y. Cadoret, S. Hervier, and D. Monceau, Oxidation of Metals, 73 (2010) 83–94.
65. V. Kucera and E. Mattson, "Atmospheric Corrosion," in *Corrosion Mechanisms*, F. Mansfield, ed., Marcel Dekker, New York, (1989) 211–284.
66. Y. Sugizaki, T. Yasunaga, and H. Sato, *Surf. Coat. Techn.*, 65 (1994) 40–44.
67. J.L. Smialek, *JOM*, January 2000, 22–26.
68. J.L. Smialek and S. Hayashi, unpublished research, (2010).
69. S. Hayashi and B. Gleeson, Oxidation of Metals, 71 (2009) 5–19.
70. R. Kircheim, X.Y. Huang, and T. Mutschele, in Hydrogen Effects on Material Behavior," N.R. Moody, W. Thompson, eds., TMS, Warrendale, PA., (1990) 85–99.
71. J. Gayda, R.L. Dreshfield, T.P. Gabb, "The Effect of Porosity and γ/γ' Eutectic Content on the Fatigue Behavior of Hydrogen Charged PWA 1480," *Scripta Met. et Mat.*, 25, (1991) 2589–2594.
72. J. Gayda, T.P. Gabb, and R.L. Dreshfield, "The Effect of Hydrogen on the Low Cycle Fatigue Behavior of a Single Crystal Superalloy," in *Hydrogen Effects on Material Behavior*, N.R. Moody, A.W. Thompson, eds., TMS, Warrendale, PA, (1990) 591–601.
73. N. Leventis, University of Missouri, Rolla, unpublished research (2005).
74. J.L. Smialek, Scripta mat., 45 (2001) 1327–1333.
75. T. Miyahara, K. Stolt, D.A. Reed, and H.K. Birnbaum, Scripta met., 19 (1985) 117–121.
76. Jayne D.T, Smialek JL. In *Microscopy of Oxidation II.* Newcomb SB, Bennett MJ, (eds). Institute of Metals: London, 1993; 183–196.
77. J.L. Smialek, Transactions ASME, 120 (1998) 370–374.
78. S. Subanovic, D. Naumenko, M. Kamruddin, G. Meier, L. Singheiser, and W.J. Quadakkers, Corr. Sci., 51 (2009) 446–450.

REPORT DOCUMENTATION PAGE			Form Approved OMB No. 0704-0188

1. REPORT DATE *(DD-MM-YYYY)*	2. REPORT TYPE	3. DATES COVERED *(From - To)*
01-04-2010	Technical Memorandum	

4. TITLE AND SUBTITLE
Moisture-Induced Alumina Scale Spallation: The Hydrogen Factor

5a. CONTRACT NUMBER

5b. GRANT NUMBER

5c. PROGRAM ELEMENT NUMBER

6. AUTHOR(S)
Smialek, James, L.

5d. PROJECT NUMBER

5e. TASK NUMBER

5f. WORK UNIT NUMBER
WBS 984754.02.07.03.16.02

7. PERFORMING ORGANIZATION NAME(S) AND ADDRESS(ES)
National Aeronautics and Space Administration
John H. Glenn Research Center at Lewis Field
Cleveland, Ohio 44135-3191

8. PERFORMING ORGANIZATION REPORT NUMBER
E-17244

9. SPONSORING/MONITORING AGENCY NAME(S) AND ADDRESS(ES)
National Aeronautics and Space Administration
Washington, DC 20546-0001

10. SPONSORING/MONITOR'S ACRONYM(S)
NASA

11. SPONSORING/MONITORING REPORT NUMBER
NASA/TM-2010-216260

12. DISTRIBUTION/AVAILABILITY STATEMENT
Unclassified-Unlimited
Subject Category: 26
Available electronically at http://gltrs.grc.nasa.gov
This publication is available from the NASA Center for AeroSpace Information, 443-757-5802

13. SUPPLEMENTARY NOTES

14. ABSTRACT
For some time the oxidation community has been concerned with interfacial spallation of protective alumina scales, not just upon immediate cool down, but as a time-delayed phenomenon. Moisture-induced delayed spallation (MIDS) and desktop spallation (DTS) of thermal barrier coatings (TBCs) refer to this process. It is most apparent for relatively adherent alumina scales that have survived initial cool down in a dry environment, have built up considerable thickness and strain energy, and have been somewhat damaged, such as by cyclic oxidation cracking. Indeed, a "sensitive zone" can be described that maximizes the observed effect as a function of all the relevant factors. Moisture has been postulated to serve as a source of interfacial hydrogen embrittlement. Hydrogen is derived from reaction with aluminum in the alloy at an exposed interface. The purpose of this monograph is to trace the close analogy of this phenomenon to other hydrogen-induced effects, such as embrittlement of aluminides and blistering of alloys and anodic alumina films. A formalized, top-down, logic-tree structure is presented as a guide to this discussion. A theoretical basis for interfacial weakening by hydrogen is first cited, as are demonstrations of hydrogen detection as a reaction product or interfacial species. Further support is provided by critical experiments that recreate the moisture effect, but by isolating hydrogen from other potential causative factors. These experiments include tests in H_2-containing atmospheres or cathodic hydrogen charging. Accordingly, they strongly indicate that interfacial hydrogen, derived from moisture, is the key chemical species accounting for delayed alumina scale spallation.

15. SUBJECT TERMS
Alumina; Heat resistant alloys; Oxidation; Hydrogen embrittlement

16. SECURITY CLASSIFICATION OF:			17. LIMITATION OF ABSTRACT	18. NUMBER OF PAGES	19a. NAME OF RESPONSIBLE PERSON
a. REPORT	b. ABSTRACT	c. THIS PAGE			STI Help Desk (email:help@sti.nasa.gov)
U	U	U	UU	37	19b. TELEPHONE NUMBER *(include area code)* 443-757-5802